Heat Transfer of the Mo-99 Research Loop

Optimising Heat Transfer of the Closed Reactor Loop Aimed at the Efficient Production of Molybdenum-99

Jurriaan A. R. Huisman

Delft University of Technology
Faculty of Applied Sciences
Department of Radiation Science Technology
Section Nuclear Energy and Radiation Applications

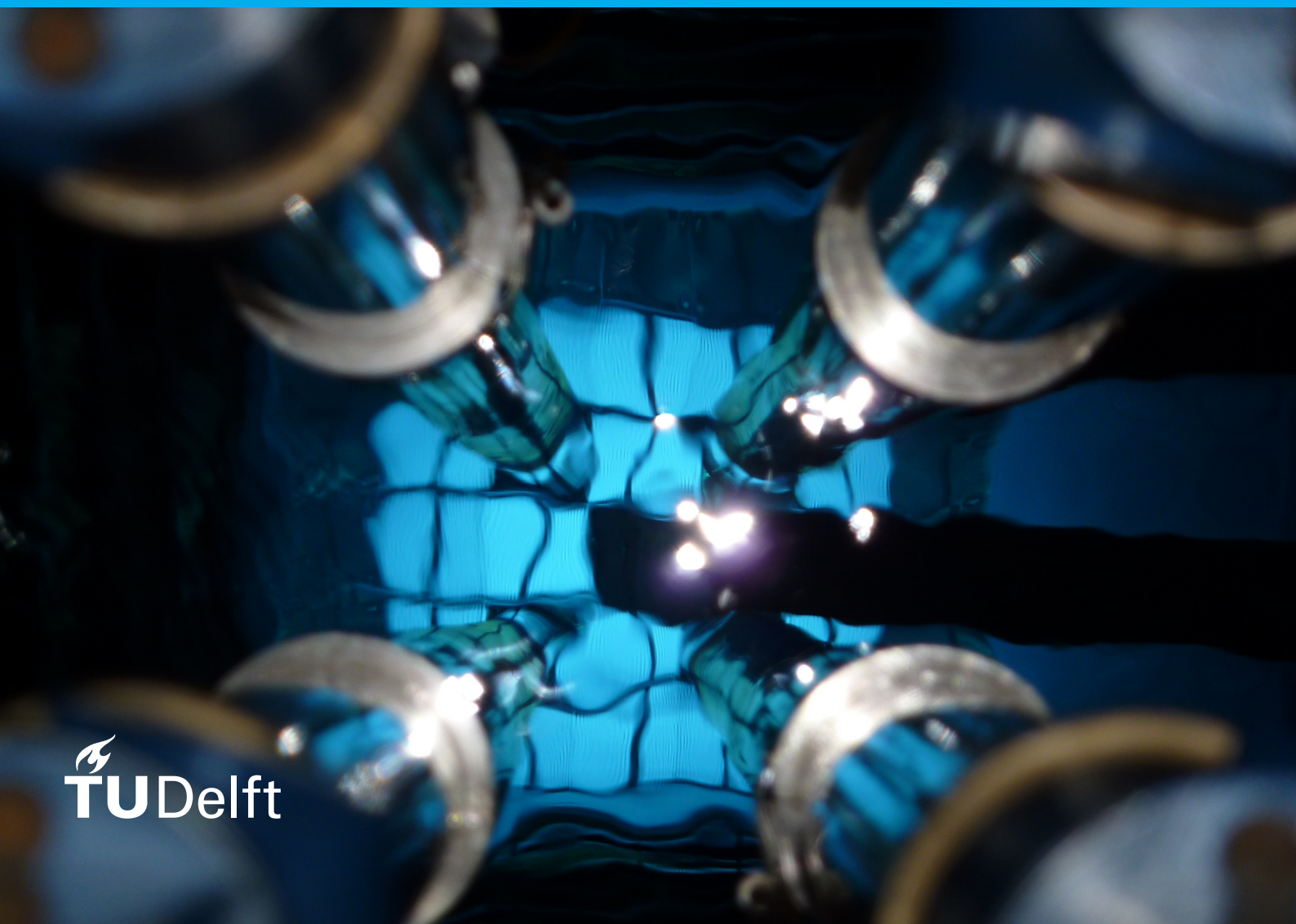

TU Delft

Heat Transfer of the Mo-99 Research Loop

Optimising Heat Transfer of the Closed Reactor Loop Aimed at the Efficient Production of Molybdenum-99

by

Jurriaan A.R. Huisman

May 27, 2016

Student number: 1307673
Faculty: Applied sciences
Department: Radiation Science Technology
Section: Nuclear Energy and Radiation Applications

Supervisors: Prof. dr. ir. J. L. Kloosterman
Dr. ir. M. Rohde

TU Delft Delft University of Technology

REACTOR INSTITUTE DELFT

Abstract

Current production methods of medical isotopes consist of intense neutron-bombardment of highly-enriched solid uranium targets, followed by rapid extraction via a chemical process. The fission of the target nuclei has a relative high yield (±6%) of molybdenum-99 (Mo-99) which is used as a source of medical isotopes. Molybdenum-99 (Mo-99) is the main source of Technetium-99m (Tc-99m), which is a short-lived metastable tracer isotope widely used in the field of diagnostic radiography.

Over the last decade the Mo-99 supply chain has suffered several disruptions. In light of the development of the Holland Particle Treatment Center (Holland PTC) and the PALLAS reactor in Petten, the Reactor Instituut Delft (RID) decided to explore different experimental setups aimed at a more efficient production of Mo-99. One of these is the implementation of a closed aqueous homogenous reactor loop in the Hoger Onderwijs Reactor (HOR). This production method uses a liquid uranyl nitrate solution, which the loop leads past a neutron source. This process is preferable over conventional methods, because it can run continuously and because the Mo-99 is relatively easy extractable from the salt solution. The research loop at the RID will function as a proof of concept for an upscaled version inside the new PALLAS reactor and will also be used as a small local Mo-99 production facility for the Holland PTC.

Previous studies have shown a substantial heat production inside the loop due to fission. This study focusses on the dissipation of that heat and the effect of different heat transfer fluids on the steady state temperature profile. It aims to determine a maximum power production that keeps the maximum temperature under $100°C$. In order to determine the temperature profiles, the setup has been modelled in COMSOL. Deuterium oxide appears to be the most effective heat transfer fluid of the fluids that have been studied.

The results show that maximum power production that keeps the temperature below $100°C$ is $1025\ W$. This model used deuterium oxide as a heat transfer fluid. The produced power roughly translates to an uranium concentration of $27.6\ g\ U\ L^{-1}$ with an enrichment level of 0.2.

Contents

1 Introduction **1**

1.1 Brief literature review . . . 1

2 Goal and outline **3**

2.1 Primary aim. . . . 3

2.2 Secondary aims. . . . 4

2.3 Outline . . . 4

3 Theoretical background **5**

3.1 Geometry . . . 5

3.1.1 Hoger Onderwijs Reactor . . . 5

3.1.2 Reactorloop . . . 6

3.2 Materials . . . 8

3.3 Transport phenomena . . . 9

3.3.1 The principle of balancing . . . 10

3.3.2 Continuity equation . . . 12

3.3.3 Navier-Stokes equations . . . 13

3.3.4 Energy and mass equations . . . 16

3.3.5 Computational Fluid Dynamics . . . 17

3.4 Heat production . . . 17

3.4.1 Fission . . . 17

3.4.2 Gamma heating. . . . 20

3.4.3 Total heat production . . . 20

3.5 Scale analysis and verification. . . . 21

4 Models and simulation in COMSOL **25**

4.1 Model definition . . . 25

4.2 Geometry . . . 27

4.3 Materials . . . 28

4.4 Heat transfer . . . 29

4.4.1 Boundaries . . . 30

4.4.2 Heat sources . . . 31

4.4.3 Radiation . . . 32

4.5 Laminar flow . . . 33

4.5.1 Boundaries . . . 33

4.5.2 Initial values . . . 33

4.6 Mesh . . . 34

5 Results **35**
5.1 Model 1: heavy water - heavy water . . . 36
5.2 Model 2: heavy water - helium . . . 38
5.3 Model 3: helium - heavy water . . . 39
5.4 Model 4: helium - helium . . . 40
5.5 Comparisons . . . 42
5.6 Notes on the concentration of uranium . . . 43

6 Conclusions and discussion **45**
6.1 Geometry . . . 45
6.2 Heat transfer fluids . . . 46
6.3 Heat production . . . 46
6.4 Uranium concentration . . . 46
6.5 Discussion . . . 46
6.6 Future research . . . 47

Bibliography **49**

Nomenclature **51**

Appendices **53**

A Verification and validation **55**
A.1 Validation . . . 56

B Flux values **57**

C MATLab code **61**
C.1 Density calculations . . . 61
C.2 Heat capacity calculations . . . 62

1 Introduction

The high flux reactor in Petten, the Netherlands, is one of few reactors in the world used for the production of medical isotopes. Petten provides around 60% of European demand and is as such an important supplier of radioactive material used for the medical diagnosis (contrast agents) and the treatment of cancer. Among others, Petten produces molybdenum-99 (Mo-99), which is an important isotope because its decay product Technetium-99m (Tc-99m) is used worldwide in over 80% of diagnostic tests involving radiopharmaceuticals.

However, the high flux reactor is ageing. In June 2014 newspapers reported growing concern about the threatening closure of the Petten reactor plant. The reactor has been closed regularly since 2002 due to a weld defect in the reactor vessel and other maintenance related issues, building up to a worldwide shortage of the isotope Mo-99 between 2008 and 2010. Its current lifespan will end around 2025.

To prevent future shortages, the foundation "Preparation Pallas reactor" (formerly a part of NRG) is developing a new reactor named PALLAS. In light of this new reactor and the development of the Holland Particle Treatment Center (Holland PTC) in Delft, the RID decided to explore different experimental setups for a closed aqueous reactor loop aimed at the efficient production of Mo-99. This production method uses a liquid uranyl nitrate solution, which the loop leads past a neutron source. This process is preferable over conventional methods, because it can run continuously and because the Mo-99 is relatively easy extractable from the salt solution. The RID plans to construct a small research loop inside the Hoger Onderwijs Reactor (HOR) as a proof of concept. If this experimental setup proves to be technically and economically appealing, an upscaled version can be realised inside the new PALLAS reactor. The researchloop could also be used as a small local Mo-99 production facility for the Holland PTC.

The feasibility of this small research loop for the HOR has been studied [1] and its potential is confirmed, but further research is required. It is suggested to read this feasibility study prior to this study.

1.1. Brief literature review

The setup considered in this study uses a uranyl nitrate salt solution with an uranium concentration of 310 $g\ U\ L^{-1}$. The uranium contains 19.75% U-235, which puts it in the high-end of low-enriched

uranium (LEU) resources. The maximum yield of the setup has been determined in [1] and amounts to 2.73mg Mo-99 per week. This is around 2.4% of the weekly worldwide demand.

The preliminary study [1] used an irradiation cycle of three hours. It theorised that shorter cycles do not allow enough time for post-processing and extraction of Mo-99. It also showed that the three hour irradiation cycle does not aversely effect the yield in comparison to shorter cycles. This study will also use three hour irradiation cycles.

2

Goal and outline

The feasibility study [1] referred to in the previous chapter contained a proposed design for a research loop which is to be placed in the DLDR beam-tube inside the HOR. This study will further investigate certain safety aspects of the proposed design. A detailed description of the geometry is given in chapter 3.

2.1. Primary aim

The primary goal of this research is to determine operating conditions for the research loop which will result in a safe steady state temperature for day-to-day operations. One of the biggest safety concerns for this setup is a potential lack of heat dissipation. Temperatures exceeding $100°C$ result in pressure buildup which can lead to potentially dangerous situations. This must be avoided and for that reason this study will investigate several aspects of the design.

In order to determine if the temperature exceeds $100°C$ this study will assess the steady state temperature field inside the setup. The temperature field inside the loop is the result of the balance between heat production due to fission and γ-heating, and heat dissipation. The heat production will first be calculated using MCNP. The results from MCNP will then be used to assess the temperature field inside the setup using the CFD simulation program COMSOL. The primary aim of this study is to evaluate the heat dissipated through conduction, convection and radiation and determining what conditions will keep the temperature below $100°C$ within the setup. The parameters that can be changed within the framework of this research are:

1. Heat transfer fluids
2. Uranium concentration
3. Construction materials

As stated earlier, the setup will be modelled and simulated using COMSOL Multiphysics. Neutron calculations on this setup were performed in MCNP by August Winkelman (RID, HOR-Development) and as such fall outside the scope of this research.

2.2. Secondary aims

The materials used for the construction of the setup are not yet determined. In order to model the setup, choices for construction materials will have to be made. This research aims to make these choices as well informed as possible.

Furthermore, the heat generated inside the setup is directly proportional to the uranium concentration, which will be proven. This study will aim to relate the temperature field inside the setup to the concentration of uranium in the fuel.

2.3. Outline

In order to model the setup and simulate the heat transfer, chapter 3 will start with a theoretical background followed by its application on this setup. Chapter 3 also discusses assumptions, relevant parameters and boundary conditions used for the simulations in COMSOL.

The models and software used to calculate the heat profile will be explained in chapter 4 and chapter 5 will present the results from the different simulations. Chapter 6 contains the conclusions, recommendations and suggestions for further research. The appendices feature an overview of the performed calculations and used data.

3

Theoretical background

Heat transfer is involved in almost every kind of physical process, and is in fact often the limiting factor for many processes. In the context of safety, heat buildup in a system can lead to an unwanted increase of pressure. This pressure increase could compromise the safety of the setup when it exceeds the maximum allowed operating pressure. By optimising heat transfer this can be avoided.

This study focuses primarily on optimising the heat transfer of the research loop. It aims to keep the maximum temperature inside the system below the boiling point of $100^{\circ}C$. This will prevent excessive pressure buildup. By calculating the temperature field inside the setup potential hot spots will be identified and the maximum temperature can be determined.

The temperature field will be calculated for normal operating conditions and abnormal conditions, as to assess how hot the system will get during day-to-day operation and in case of a malfunction. This chapter will start with an overview of the setup and the reactor core, followed by a brief summary of the physics used for this problem and its application on this setup.

3.1. Geometry

The subject of this study is a research loop aimed at an efficient production of molybdenum-99. This loop will be an U-shaped pipe placed within the DLDR beam-tube (see figure 3.1) inside the reactorpool of the "Hoger Onderwijs Reactor".

3.1.1. Hoger Onderwijs Reactor

The "Hoger Onderwijs Reactor" (HOR) is a 2 MW pool-type research reactor operated by the Reactor Instituut Delft which is part of the faculty of Applied Sciences of Delft University of Technology. The HOR is used as neutron source for various research purposes. It is powered by low-enriched uranium-235 (< 20%) and uses an MTR-fuel assembly. The core is composed of twenty fuel assemblies and four control assemblies. There are three beam-tubes running through the reactor core, which are mainly used for neutron scattering experiments. There is also a fourth beam-tube present, the DLDR, which runs tangential past the reactor-core (past the backside of the core in figure 3.1).

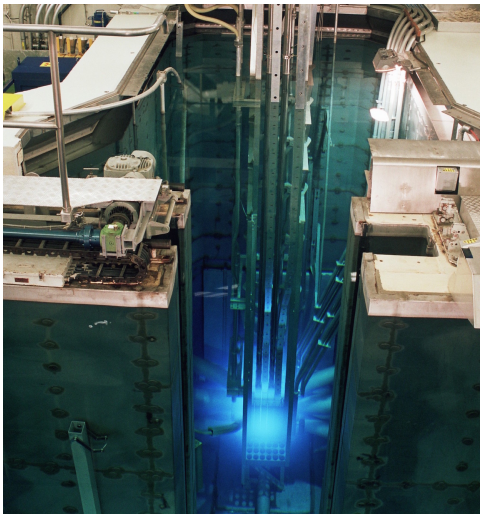

Figure 3.1: Reactor core

3.1.2. Reactorloop

The subject of this study, the reactor loop, will be placed inside the DLDR beam-tube. The loop will be U-shaped and contains a uranium salt solution which will be pumped through the loop. During its stay in the loop, the uranium salt will be irradiated by neutrons from the reactor core. A small percentage, around 6.1%, of the fission events will lead to the production of Mo-99 [2].

Figure 3.2 shows the topview of the reactor basin and the DLDR beam-tube highlighted in red. The U-tube will be placed inside this beam-tube. The blue represents the water of the reactorpool and on the left a floodgate is indicated in dark grey. The concrete construction of the bassin is represented by the striped area.

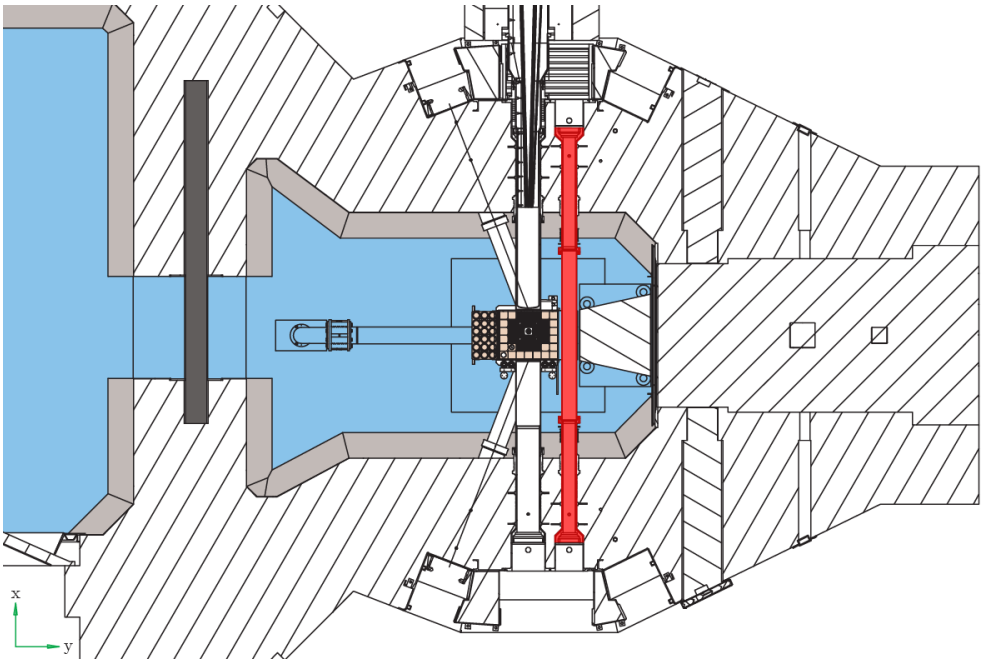

Figure 3.2: Schematic topview of reactor core and pool

Elgin [1] decided upon a U-shaped loop, because it lengthens irradiation times, and because the entrance to the DLDR is blocked on one side (the upper entrance in figure 3.2 to the DLDR is blocked). The design has the additional advantage that it also restricts the space needed for pre- and post-processing of the fuel. This research will study the same design. The diameter of the loop piping will be made as large as possible in order to maximise the yield of the setup [1]. The DLDR beam-tube has an inner-diameter of $140mm$ and has a wall thickness of $5mm$. For safety reasons this tube will contain an additional second tube which will function as a flood barrier in case of a leakage in the outer DLDR (indicated in red in figures 3.3 and 3.4). This barrier has an outer diameter of $114mm$ and inner diameter of $108mm$. The reason for the much smaller diameter of the secondary barrier is the Boron radiation shielding present at the openings of the DLDR. The Boron shielding is present to minimise the neutron damage to the stainless steel connectors present in the reactorpool wall.

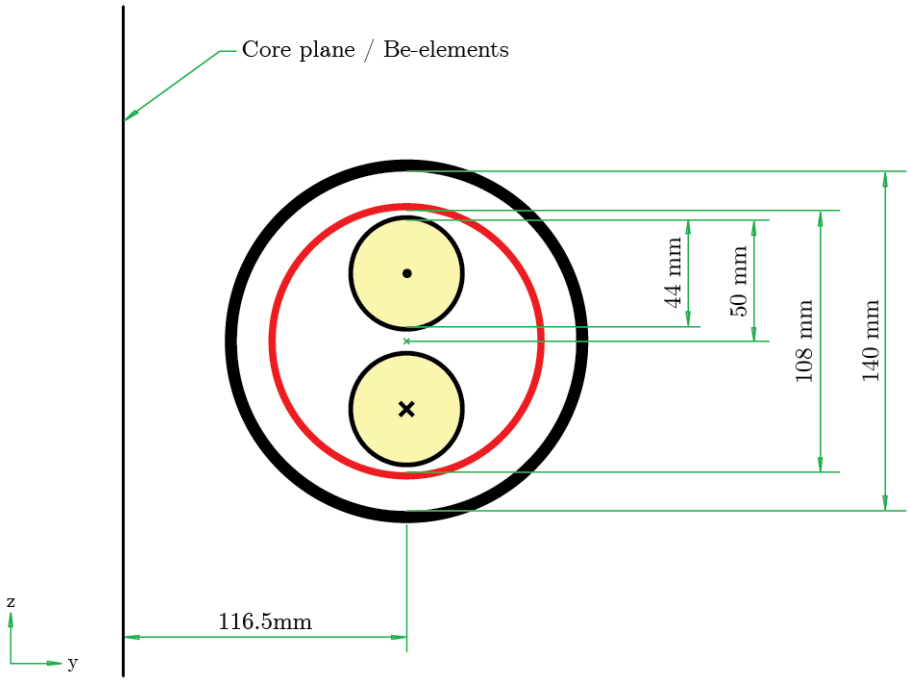

Figure 3.3: Cross section of setup with diameters

In order to maximise the Mo-99 yield, the diameter of the loop is maximised [1]. The piping of the loop has an outer-diameter of $48mm$ and an inner-diameter of $44mm$. The centers of both legs of the loop are a distance $56mm$ apart. This makes the smallest space between the loop and the inner flood barrier $2mm$. The orientation of the loop is upright, meaning the two legs of the loop are placed on top of one another, see figure 3.3. This is beneficial for the Mo-99 production [1]. Figure 3.3 gives a schematic overview of the setup and its diameters.

The path of the DLDR beam-tube runs through the concrete structure and the reactor pool, and consists of different parts, as is depicted in figure 3.2. The part of interest to this study is the central part, which is made of $AlMg_3$, an aluminum alloy. The other parts are made of an Iron alloy. Aluminum alloys are almost completely transparent to neutrons, in contrary to iron alloys. Since the neutron-uranium interactions are the source of heat in this problem, this study will confine the calculations to this central part of the tube. This part will hence be referred to as the DLDR beam-tube.

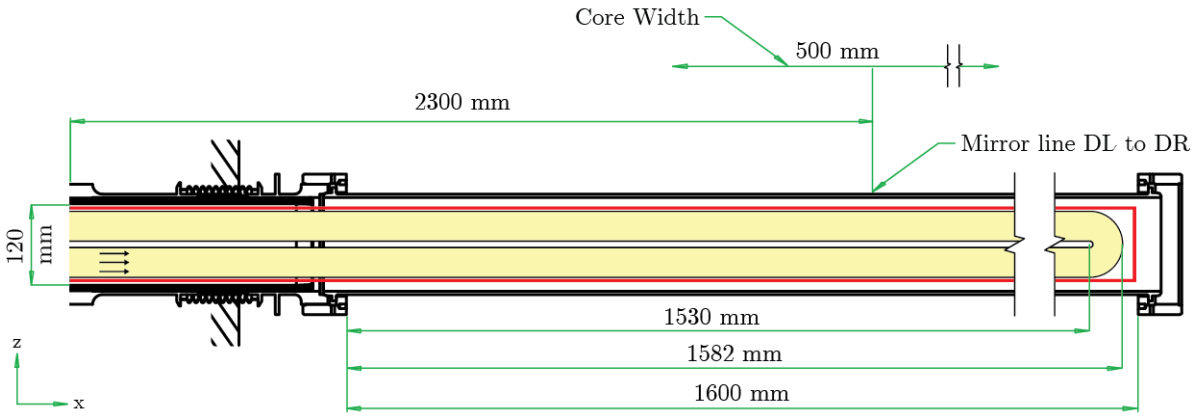

Figure 3.4: Cross section of setup

The beam-tube has a total length of 1600mm and is currently sealed at both ends by use of a flange. These flanges function as secondary flood barriers in case of a leakage. In order to maintain this function, one of these will be replaced by a cylinder. This cylinder is closed off at one side and will cover the length of the inside of the DLDR (indicated in red in figure 3.4). The loop itself will be placed inside the cylinder. The 2300mm length is the distance from one of the openings of the DLDR to the mirror plan of the beam-tube.

3.2. Materials

This section will briefly cover the different materials best suited for the setup. As stated earlier the DLDR beam-tube is made from $AlMg_3$. An aluminum alloy with excellent structural and thermo-physical properties, which is almost completely transparent to neutrons and it has a low neutron activation.

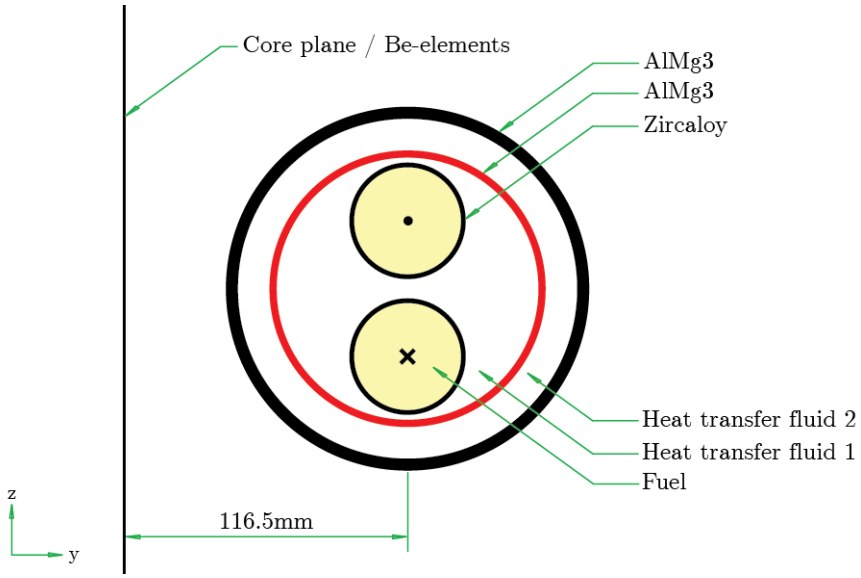

Figure 3.5: Cross section of setup with materials

The fuel used in the loop is an uranyl nitrate solution, which has a high acidity [1]. The corrosion

resistance of $AlMg_3$ is very poor, so using this for the loop is impossible. Zircaloy, an alloy of zirconium, has excellent corrosion resistance [4] and has a low neutron absorption cross section, around 0.18 $barn$ [5]. This makes it very suitable for nuclear applications.

The space between the DLDR and the secondary flood barrier and the space between the inner flood barrier and the U-tube will be filled with a heat transfer fluid as depicted in figure 3.5. It is preferable to choose a heat transfer fluid with a high thermal conductivity λ since this will benefit heat transfer. Normally this would mean choosing a liquid instead of a gas, however liquids often act as a moderator causing a lower neutron flux, which is undesirable. As of yet it is unclear if this decrease in the neutron flux will be a limiting factor, so the temperature field calculations will be performed for both liquids and gasses.

Since a large neutron flux is preferable inside the reactor loop, the heat transfer fluids need a small total neutron cross section. Deuterium oxide, commonly known as heavy water, has a relative small neutron cross section when compared to normal water [6] and has similar thermal properties. This makes it a suitable choice.

Gasses are, due to their much lower density, often transparent to neutrons. So the choice for a suitable gas is solely based on the thermophysical properties. The data companion shows that helium [7] has the highest thermal conductivity. Hydrogen has a similar conductivity, but helium is the safer choice since it is an inert gas.

COMSOL has an extensive material library that was used for all material properties. However, as of yet this database does not hold the physical properties of uranyl nitrate solutions. In fact, there is no extensive database with properties of uranyl nitrate solutions, so whenever thermal properties of uranyl nitrate were not available they were replaced with the properties of water. This has been done throughout this research. This is an acceptable substitution, because properties of the uranyl nitrate solution are comparable to the thermal properties of water for low concentrations [3]. Table 3.1 gives an overview of the used properties of uranyl nitrate solution.

Property	Value	Water property used?
Dynamic viscosity	$1.09 \cdot 10^{-3} [Pa \cdot s]$	no
Specific heat	$2.72 \cdot 10^{3} [Jkg^{-1}K^{-1}]$	no
Thermal conductivity	COMSOL library	yes
Thermal expansion coefficient	COMSOL library	yes
Reference temperature	$336.15K$	yes

Table 3.1: Relevant material properties of uranyl nitrate solution

3.3. Transport phenomena

The field of transport phenomena describes the transfer of momentum, energy and mass in the form of mathematical relations. These relations are a result of the laws of conservation of momentum, energy, and mass combined with the laws that describe the fluxes of these conserved quantities. The relations between these quantities can be used to solve eg. the temperature field inside a system. The most accurate way of describing these relations is in the form of a set of differential equations which have to be solved simultaneously.

This set of equations consists of the continuity equation (3.1), the Navier-Stokes equations (3.2), and the equations that describe the transfer of energy (3.3) and mass (3.4). These have to be solved si-

multaneously because they form a mutually dependent system of differential equations. The equations are defined as follows:

$$\frac{\partial \rho}{\partial t} = -\nabla \cdot (\rho \vec{v}) \tag{3.1}$$

$$\rho \frac{\partial \vec{v}}{\partial t} + \rho \vec{v} \cdot \nabla \vec{v} = \mu \nabla^2 \vec{v} - \nabla p + \rho \vec{g} \tag{3.2}$$

$$\rho \frac{\partial c_p T}{\partial t} + \rho \vec{v} \cdot \nabla (c_p T) = \lambda \nabla^2 T + q \tag{3.3}$$

$$\frac{\partial c}{\partial t} + \vec{v} \cdot \nabla (c) = \mathbb{D} \nabla^2 c + r \tag{3.4}$$

Since the literature on this subject is extensive [8], [9], the next sections will contain only a brief derivation of this set of differential equations. Furthermore the derivation followed uses a more physical and intuitive approach. This derivation might not be correct for the general case, but the resulting set of equations certainly holds for all situations.

3.3.1. The principle of balancing

As stated before, the above equations follow from the laws of conservation. When working with a conserved quantity G it is convenient to balance inflow, outflow and production of the quantity over the volume of interest. Figure 3.6 gives a graphical representation of this balance:

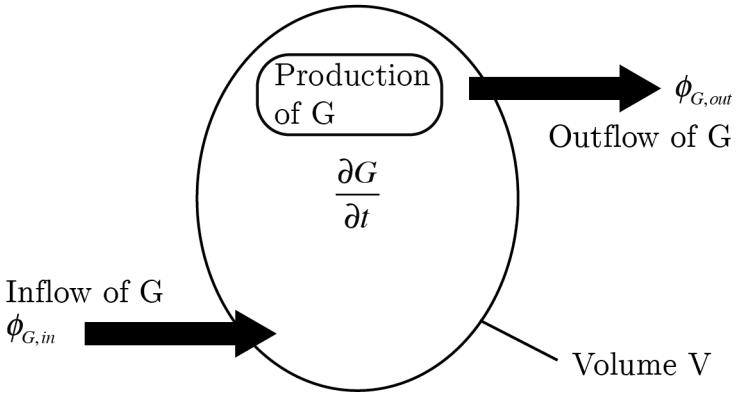

Figure 3.6: General balance

The general form of such a balance is:

$$\frac{dG}{dt} = \phi_{G,in} - \phi_{G,out} + P_G \tag{3.5}$$

- $\frac{dG}{dt}$ represent the change of the quantity G inside the volume V over time and is called the accumulation term.
- $\phi_{G,in}$ and $\phi_{G,out}$ represent the inflow and outflow of the quantity G. A flow is also known as a flux and is denoted by ϕ
- P_G represents the production of the quantity G inside the volume V.

This balance needs to hold for all sizes of the volume V. When considering a large volume, Akker[8] dubs balance (3.5) a macrobalance and when working with a tiny volume a microbalance.

Balance (3.5) also holds for all quantities. When looking at the transport of energy for instance, the balance contains all the energy entering the system, exiting the system and the production of energy. (Heat is not used here, because it is not a conserved quantity. Instead, the conserved quantity is the total energy. This means there is both a heat flux and a energy flux. These are alike but often not identical.)

Before applying equation (3.5) to any quantity it is useful to make a clear distinction. Energy, mass, and momentum can basically be transported in two different ways. As a result of collective movement of molecules and through individual molecule movement. The fluxes resulting from the collective behaviour are forms of convective transfer.

Individual molecules are also capable of transferring energy, mass, and momentum through movement and interaction. Before moving on to the derivation of equations (3.1) - (3.4), it is convenient to give a short description of the molecular transport phenomena for energy, mass, and momentum.

3.3.1.1 Transfer of energy

The transfer of thermal energy through conduction is described by Fourier's law. Conduction is the ability of molecules to transport heat without transporting mass. Fourier's law [8] connects the heat flux and the driving temperature gradient as follows:

$$\phi''_q = -\lambda \nabla T \tag{3.6}$$

- ϕ''_q is the heat flux density $\left[W \cdot m^{-2}\right]$
- λ is the thermal conductivity $\left[W \cdot m^{-1} \cdot K^{-1}\right]$
- ∇T is the temperature gradient $\left[K \cdot m^{-1}\right]$

In words, the law states that a temperature gradient in any direction will cause a heat flux, and that this heat flux will flow from a place with a high temperature to a place with a low temperature. This last part is indicated by the minus sign in equation (3.6).

3.3.1.2 Transfer of mass

The molecular transfer of mass, or diffusion, is the movement of molecules as a result of a concentration gradient in a certain region. In other words, it is the net movement of molecules from a domain with a high concentration to a domain with a low concentration. The mathematical expression of this relation is known as Fick's law [8]. According to Fick, the mass transported of a substance A in a fluid through diffusion is equal to:

$$\phi''_m = -\mathbb{D} \nabla c \tag{3.7}$$

- ϕ''_q is the mass flux density $\left[mol \cdot m^{-2} \cdot s^{-1}\right]$
- $\mathbb{D}$ is the diffusion coefficient $\left[m^2 \cdot s^{-1}\right]$
- c is the concentration $\left[mol \cdot m^{-3}\right]$

3.3.1.3 Transfer of momentum

According to Newton [8], the shear tension τ_{yx} in a newtonian fluid with a laminar flow is directly related to the dynamic viscosity μ of the fluid and the velocity gradient perpendicular to the flow direction:

$$\tau_{yx} = -\mu \frac{\partial v_x}{\partial y} \tag{3.8}$$

- τ_{yx} is the shear stress $\left[N \cdot m^{-2}\right]$
- μ is the dynamic viscosity $\left[N \cdot s \cdot m^{-2}\right]$
- v_x is the velocity $\left[m \cdot s^{-1}\right]$

This transfer of momentum is a result of collisions of molecules within the fluid. With each collision molecules exchange momentum.

3.3.1.4 Radiation

Radiation is the transfer of heat by electromagnetic waves, or photons. It stands apart, because it is independent of heat transfer by convection and conduction. Every solid body constantly emits radiation, the rate at which it emits energy is directly related to its temperature. For a perfect black body radiator, the amount of energy dissipated is equal to the Stefan-Boltzman equation [8]:

$$\phi_q'' = \sigma T^4 \tag{3.9}$$

- ϕ_q is the heat flux density $\left[W \cdot m^{-2}\right]$
- σ Stefan-Boltmann constant 5.67 10^{-8} $\left[W \cdot m^{-2} \cdot K^{-4}\right]$
- T is the temperature of the body $[K]$

However this law is only applicable to perfect black body radiators and in practice only very few are. To solve this problem the emission coefficient e was introduced. It is a dimensionless coefficient and has a value between 0 and 1. It represents to what degree a body resembles a black body. Combining this with equation (3.6) gives a general expression for the heat dissipated through radiation:

$$\phi_q'' = e\sigma T^4 \tag{3.10}$$

3.3.2. Continuity equation

As stated in paragraph 3.3.1, equation (3.5) needs to hold for all volume sizes. The continuity equation is a result of the mass conservation law and will be derived using the cubic volume element method. The derivation given here is identical to the one found in [8]. Using a total mass balance an expression can be derived that must hold for every flow field. Consider a tiny cubical reference volume V inside a time dependent fluid flow with size $dxdydz$.

The microbalance for this volume V contains an accumulation term and six mass transfer terms, one for each surface of the cube. The accumulation term is equal to:

$$\frac{\partial \rho}{\partial t} dxdydz \tag{3.11}$$

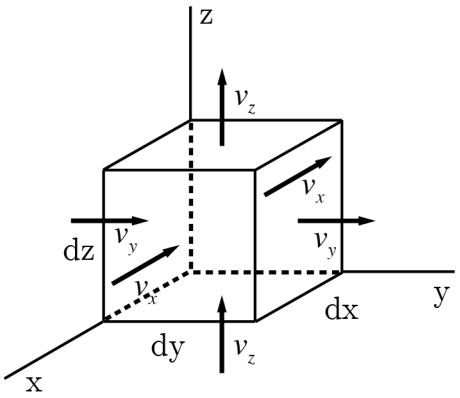

Figure 3.7: Cubical volume V

The mass transported through the front face due to convection:

$$[\rho v_x]_{x,y,z} dydz$$

As a result of the velocity v_x mass is also transported through the back of the cubical volume:

$$[\rho v_x]_{x+dx,y,z} dydz$$

Adding these gives the total contribution to convective mass transport in the x-direction:

$$[\rho v_x]_{x,y,z} dydz - [\rho v_x]_{x+dx,y,z} dydz = -\frac{\partial}{\partial x}(\rho v_x) dxdydz \tag{3.12}$$

Similar expression can de derived for the left, right, up and bottom planes, by balancing the inflow and outflow of mass:

$$[\rho v_y]_{x,y,z} dxdz - [\rho v_y]_{x,y+dy,z} dxdz = -\frac{\partial}{\partial y}(\rho v_y) dxdydz \tag{3.13}$$

$$[\rho v_z]_{x,y,z} dxdy - [\rho v_z]_{x,y,z+dz} dxdy = -\frac{\partial}{\partial z}(\rho v_z) dxdydz \tag{3.14}$$

Combining equations (3.11),(3.12), (3.13), and (3.14) and dividing by the volume size of the cube $dxdydz$ results in the so called continuity equation:

$$\frac{\partial \rho}{\partial t} = -\nabla \cdot (\rho \vec{v}) \tag{3.15}$$

This result is equal to equation (3.1).

3.3.3. Navier-Stokes equations

The Navier-Stokes equations describe the motion of a fluid and arise, in this derivation, from applying Newton's second law to fluids. They will be derived using the microbalances for transfer of

momentum. Before deriving this set of differential equations it is useful to define momentum in the context of a fluid. The velocity $\vec{v}$ can be viewed as concentration of momentum in the direction of the flow. Therefore $\rho\vec{v}$ can be seen as the momentum concentration per volume unit.

The velocity field $\vec{v}$ in a volume is the result of a redistribution of the momentum inside the volume of interest, while forces act on the edges of the domain and on the mass inside the domain. As in the previous paragraph, the cubic volume element method will be used to balance the momentum and forces acting on the volume.

Consider again the volume from figure 3.7. Due to the fact that both momentum and force are vectors, the momentum balance needs to be formulated separately for the x, y, and z-direction. First up is the x-direction.

The momentum microbalance for the x-component of the flow has multiple terms accounting for accumulation, convective transfer, molecular transfer, and production.

Accumulation
The accumulation term is equal to:

$$\frac{\partial \rho v_x}{\partial t} dxdydyz \tag{3.16}$$

Convective transfer
The velocity vector $\vec{v}$ can be factorised into x,y, and z components. So the concentration of momentum in the x-direction flowing through the front face is equal to ρv_x. This means the total convective transfer of momentum in the x-direction through this plane is:

$$[v_x \rho v_x]_{x,y,z} dydz$$

Momentum exiting the cubic volume through the back face is equal to:

$$[v_x \rho v_x]_{x+dx,y,z} dydz$$

Where the momentum concentration in x and $x+dx$ differ. Combining inflow and outflow in the x-direction gives a net contribution to the accumulation of x-momentum:

$$[v_x \rho v_x]_{x,y,z} dydz - [v_x \rho v_x]_{x+dx,y,z} dydz = -\frac{\partial}{\partial x}(v_x \rho v_x) dxdydz \tag{3.17}$$

Contributions to the accumulation term of x-momentum as a result of flow in the y-direction and the z-direction can be derived in a similar fashion resulting in:

$$-\frac{\partial}{\partial y}(v_y \rho v_x) dxdydz \tag{3.18}$$

$$-\frac{\partial}{\partial z}(v_z \rho v_x) dxdydz \tag{3.19}$$

Molecular transfer
When dealing with a newtonian fluid, the contribution to the x-momentum by the shear stress on the left face is defined by newton's law (3.8) and is equal to:

$$\left[-\mu \frac{\partial v_x}{\partial y}\right]_{x,y,z} dxdz$$

The contribution to the x-momentum by the shear stress on the right face is:

$$-\left[-\mu\frac{\partial v_x}{\partial y}\right]_{x,y+dy,z} dxdz$$

So the net contribution to the accumulation of the momentum flux in the x-direction is:

$$\left(\left[-\mu\frac{\partial v_x}{\partial y}\right]_{x,y,z} dxdz\right)-\left(\left[-\mu\frac{\partial v_x}{\partial y}\right]_{x,y+dy,z} dxdz\right)=\frac{\partial}{\partial y}\left(\mu\frac{\partial v_x}{\partial y}\right)dxdydz \tag{3.20}$$

Again, similar expressions can be derived for the momentum flux in the x-direction through the the other faces of the cubical volume:

$$\frac{\partial}{\partial x}\left(\mu\frac{\partial v_x}{\partial x}\right)dxdydz \tag{3.21}$$

$$\frac{\partial}{\partial z}\left(\mu\frac{\partial v_x}{\partial z}\right)dxdydz \tag{3.22}$$

For the derivation of the molecular terms Akker [8], assumed that the shear tension only occurs perpendicular to the flow direction, because this allows the use of Newton's law (3.8). This representation is an incorrect simplification. Making the derivation somewhat oversimplified. The result however is correct.

Production
Momentum will be generated due to all forces acting on the volume. The x-component of the flow will only exert a pressure on the front and back faces of the cubical volume, so its contribution is equal to:

$$[p]_x dydz-[p]_{x+dx} dydz=-\frac{\partial p}{\partial x}dxdydz \tag{3.23}$$

The momentum generated due to x-component of gravity working on the volume is:

$$g_x\rho dxdydz \tag{3.24}$$

Combining equations 3.16 - 3.19, 3.21 - 3.24 and dividing by $dxdydz$ yields:

$$\begin{aligned}\frac{\partial \rho v_x}{\partial t}=&-\frac{\partial}{\partial x}(v_x\rho v_x)-\frac{\partial}{\partial y}(v_y\rho v_x)-\frac{\partial}{\partial z}(v_z\rho v_x)+\\&+\frac{\partial}{\partial x}\left(\mu\frac{\partial v_x}{\partial x}\right)+\frac{\partial}{\partial y}\left(\mu\frac{\partial v_x}{\partial y}\right)+\frac{\partial}{\partial z}\left(\mu\frac{\partial v_x}{\partial z}\right)-\frac{\partial p}{\partial x}+g_x\rho\end{aligned} \tag{3.25}$$

Rewriting this equation by making use of $\frac{\partial \rho v}{\partial t}=\rho\frac{\partial v}{\partial t}+v\frac{\partial \rho}{\partial t}$ leads to:

$$\begin{aligned}&\rho\frac{\partial v_x}{\partial t}+\rho v_x\frac{\partial v_x}{\partial x}+\rho v_y\frac{\partial v_x}{\partial y}+\rho v_z\frac{\partial v_x}{\partial z}=\\&=\mu\left(\frac{\partial^2 v_x}{\partial x^2}+\frac{\partial^2 v_x}{\partial y^2}+\frac{\partial^2 v_x}{\partial z^2}\right)-\frac{\partial p}{\partial x}+\rho g_x\end{aligned} \tag{3.26}$$

Similar equations can de derived for the y and z-component of the fluid which will lead to equations of motion for momentum in y-direction and z-direction:

$$\begin{aligned}\rho\frac{\partial v_y}{\partial t}+\rho v_x\frac{\partial v_y}{\partial x}+\rho v_y\frac{\partial v_y}{\partial y}+\rho v_z\frac{\partial v_y}{\partial z}=\\ =\mu\left(\frac{\partial^2 v_y}{\partial x^2}+\frac{\partial^2 v_y}{\partial y^2}+\frac{\partial^2 v_y}{\partial z^2}\right)-\frac{\partial p}{\partial y}+\rho g_y\end{aligned} \tag{3.27}$$

$$\begin{aligned}\rho\frac{\partial v_z}{\partial t}+\rho v_x\frac{\partial v_z}{\partial x}+\rho v_y\frac{\partial v_z}{\partial y}+\rho v_z\frac{\partial v_z}{\partial z}=\\ =\mu\left(\frac{\partial^2 v_z}{\partial x^2}+\frac{\partial^2 v_z}{\partial y^2}+\frac{\partial^2 v_z}{\partial z^2}\right)-\frac{\partial p}{\partial z}+\rho g_z\end{aligned} \tag{3.28}$$

Equations (3.26), (3.27), and (3.28) are commonly known as the Navier-Stokes equations and describe the motion of fluids. In vector notation these combine to:

$$\rho\frac{\partial\vec{v}}{\partial t}+\rho\vec{v}\cdot\nabla\vec{v}=\mu\nabla^2\vec{v}-\nabla p+\rho\vec{g} \tag{3.29}$$

In this form the equation is equal to equation (3.2). The Navier-Stokes equations have a great range of practical uses from studying laminar flow through a pipe to modelling turbulent air flow around an aircraft. It has not yet been proven that solutions to the equations in 3 dimensions always exist (one of the Millennium Prize Problems), but as yet, no counter example has been found.

3.3.4. Energy and mass equations

In a similar way, by using the cubic volume element method and setting up the microbalance for thermal energy and mass tranfer, the general equations for heat and mass transfer can be obtained. For a detailed derivation please see [8] and [9]. The heat equation is equal to:

$$\begin{aligned}\rho\frac{\partial c_pT}{\partial t}+\rho v_x\frac{\partial c_pT}{\partial x}+\rho v_y\frac{\partial c_pT}{\partial y}+\rho v_z\frac{\partial c_pT}{\partial z}=\\ =\lambda\left(\frac{\partial^2 T}{\partial x^2}+\frac{\partial^2 T}{\partial y^2}+\frac{\partial^2 T}{\partial z^2}\right)+q\end{aligned} \tag{3.30}$$

and the equation for the transfer of mass:

$$\begin{aligned}\frac{\partial c}{\partial t}+\rho v_x\frac{\partial c}{\partial x}+\rho v_y\frac{\partial c}{\partial y}+\rho v_z\frac{\partial c}{\partial z}=\\ =\mathbb{D}\left(\frac{\partial^2 c}{\partial x^2}+\frac{\partial^2 c}{\partial y^2}+\frac{\partial^2 c}{\partial z^2}\right)+r\end{aligned} \tag{3.31}$$

The similarities between equations (3.26) - (3.28), (3.30), and (3.31) are evident and illustrate the analogy between the transfer of mass, energy and momentum. In combination with the continuity equation (3.15) and sufficient boundary values, these relations form a set of differential equations that can be used to evaluate all quantities as a function of time and space.

Note that in vector notation equations (3.30), and (3.31) are equal to equations (3.3) and (3.4).

3.3.5. Computational Fluid Dynamics

The system of equations derived in the previous paragraphs can only be solved analytically for symmetrical problems that have a reduced degrees of freedom. For more complicated problems, such as the temperature field inside the research loop, the system of equations needs to be solved numerically. The field of computational fluid dynamics specifically aims to solve these equations using numerical methods.

There are different software packages available for CFD-simulations. This study uses COMSOL Multiphysics, which uses a finite element method to find an approximation to the solution of the problem.

3.4. Heat production

There are two significant contributors to the heat production inside the loop: fission and gamma heating. Fission is the process of splitting heavy nuclei into smaller fragments via neutron interaction. This process is accompanied by a substantial release of energy. These fission events also occur in the fuel inside the loop, where 6 % of these events lead to the production of Molydenum-99.

3.4.1. Fission

Fission of a uranium nucleus by a neutron releases around $200 MeV$ of energy [11]. A simple multiplication of this energy production and the number of fission events, or the reaction rate, results in the total heat production inside the loop.

The reaction rate depends on the neutron flux, the concentration of uranium in the fuel, and the neutron interaction cross section. These will have to be determined. The neutron flux calculations for this setup were performed by August Winkelman (RID, HOR-Development) using the Monte Carlo N-Particle 6.1 code (or MCNP6.1) developed by the Los Alamos National Laboratory.

MCNP6.1 has two outputs, the first is the neutron flux inside the loop. The calculations showed only minor variations in the flux in the z-direction. In the y-direction, the neutron and gamma flux densities will decrease as a result of self-shielding as they pass through the setup. This gradient in the flux between the side facing the core and the opposite side will result in a similar gradient in the heat production. MCNP accounts for the effect of self-shielding in its calculations of the flux densities and outputs an average flux. For ease of calculation, this report uses the average flux inside the loop and considers the flux constant in both the z- and y-directions.

The biggest change in the flux density was found to be along the x-direction. Figure 3.8 shows the flux density as a function of x-coordinate as well as a zx-plane cross section of the setup as a reference. It shows that the neutron flux is highest closest to the core and that the flux rapidly declines with increasing distance.

The total neutron flux is divided in three different energy groups in the graph in figure 3.8. The lines in 3.8 represent the fluxes belonging to the different groups. The energy intervals are defined in the legend. The heat produced in the loop will mainly be caused by thermal neutron fission of uranium-235, ie. neutrons within the energy range [0 - 625 eV]. This is due to the fact that uranium-238 is not a fissile material. It is fissionable by fast neutrons, but that contribution is very small.

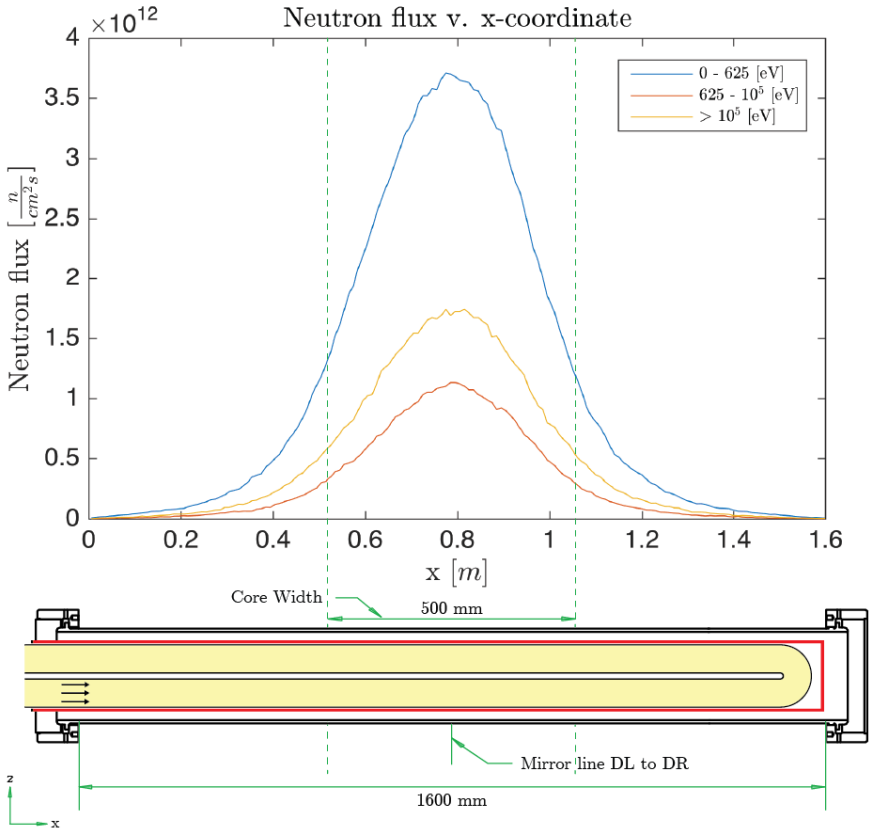

Figure 3.8: Neutron flux density inside loop along the x-direction and a schematic cross section of the setup

As mentioned earlier, the reaction rate is a function of the neutron flux, uranium density, and neutron cross section. This study assumes a uniform concentration throughout the loop. This will result in a slightly higher heat production, which will lead to a conservative estimate of the temperature field. For ease of calculation the uranium-235 molar density will be determined using the concentration and the molar mass. The molar concentration is defined as:

$$c_{mol} = \frac{c}{M} \tag{3.32}$$

Where c is the concentration of the solution and M is the molar mass of the uranyl nitrate $[UO_2(NO_3)_2]$. Since uranyl nitrate only has one uranium atom, the number of uranium atoms within a volume V is subsequently given by:

$$N = c_{mol} N_A \tag{3.33}$$

The reaction rate is defined by Duderstadt [11] as:

$$R''' = \varepsilon \sigma \phi_n N \tag{3.34}$$

- ε is the level of enrichment
- σ is the microscopic neutron cross section $[b]$
- ϕ_n is the neutron flux $\left[m^{-2} \cdot s^{-1}\right]$
- N is the number of atoms per volume $\left[m^{-3}\right]$

All of these quantities are known, except for the neutron cross section. The thermal neutron cross section of uranium-235 for fission events is on average 583 b [6]. Where b stands for $barn$ which is

a typically used unit of area for cross sections. A barn is defined as $10^{-28}\ m^2$ and is approximately the cross-sectional area of an uranium nucleus.

	thermal cross section $[barn]$	fast cross section $[barn]$
u-235	583	1
u-238	0.00002	0.3

These cross sections in combination with the neutron flux distribution show that the only significant contribution to the heat production is due to uranium-235 fission events. Since every fission event releases around $200 MeV$ of energy, the heat production per volume, or produced power per volume, is given by:

$$P''' = ER''' \tag{3.35}$$

- P''' is the power production per volume $\left[W \cdot m^{-3}\right]$
- E is the amount of released energy per fission event, which is 200 MeV $[eV]$
- R''' is the reaction rate $\left[m^{-3} \cdot s^{-1}\right]$

Equation 3.35 can be plotted as a function of the y-coordinate of the loop. Figure 3.9 shows this power distribution (this figure used a slightly modified version of equation 3.35 as will be explained in section 3.4.3).

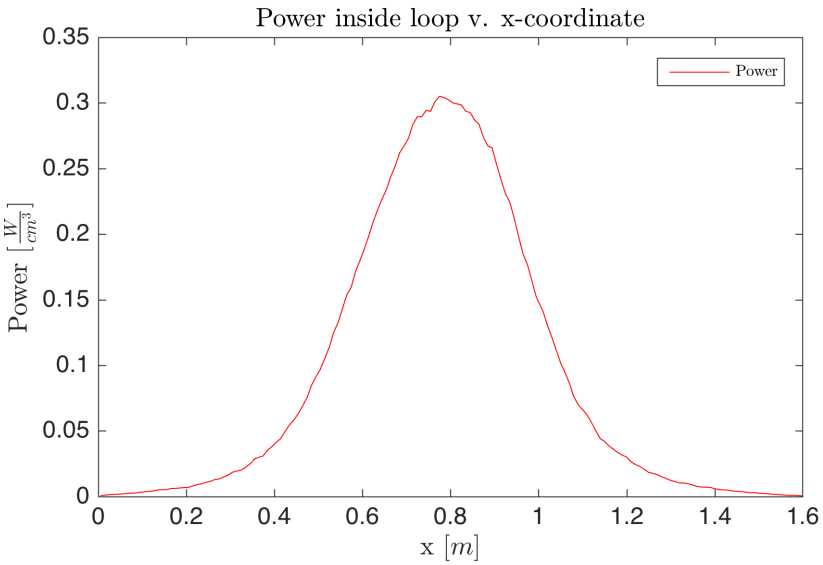

Figure 3.9: Power distribution inside the fuel due to fission

The total heat production within the fuel is obtained by integrating equation 3.35 over the entire volume of the loop:

$$P_{fuel} = \iiint_{V_{fuel}} ER'''\, dx\, dy\, dz \tag{3.36}$$

The above described method allows us the make an estimation of the heat production inside the fuel during operation due to fission. This was found to be around: $7.16 kW$ using a uranium concentration of $310 g\ U\ L^{-1}$. The heat production due to fission was also calculated more accurately in MCNP. These calculations showed the generated heat to be: $7.87 kW$ using the same concentration.

3.4.2. Gamma heating

Gamma heating is the other big contributor to the heat production inside the setup. It is caused by the interaction of gamma particles with construction materials of the setup. The interactions result in a deposition of energy onto the material, which increases the material temperature.

The section HOR Development uses a rule of thumb of approximately 0.3 W/g for gamma heating of all construction materials close to the reactor core [12]. An estimation of the total amount of energy deposited by gamma particles on the loop and inner flood barrier can be made using this number:

$$P = \iiint_{V_{mat}} u\rho \, dx\, dy\, dz \tag{3.37}$$

- P is the power production $[W]$
- u is the energy density used by the department of HOR Development $\left[W \cdot g^{-1}\right]$
- ρ is the material density $\left[W \cdot g^{-1}\right]$

3.4.3. Total heat production

MCNP calculates the total heat production for the setup caused by fission as well as energy deposition as a result of gamma radiation. It does not provide a power distribution, but the outputs can be used as a convenient check.

In practice however, these values were used as a benchmark. The heat production and energy deposition calculated by MCNP are more accurate than the estimations made in the previous sections. This is because, among other things, they account for fission of uranium-238 and the curvature of the gamma flux for gamma heating, which were neglected in the estimations. Since the thermal neutron and gamma fluxes are the primary cause of heating, their power distributions will be identical in shape to these fluxes. The heat generated by fission and the energy deposition can therefore be written as a function of these fluxes:

$$P_{fission} = \iiint_{V_{fuel}} E\alpha\varepsilon\sigma\phi_n c_{mol} N_A \, dx\, dy\, dz \tag{3.38}$$

$$P_{deposition} = \iiint_{V_{mat}} \beta\phi_\gamma \, dx\, dy\, dz \tag{3.39}$$

Where α and β are constants. The value of α in equation 3.38 was varied to match $P_{fission}$ to the calculated value in MCNP for fission heating ($7.87kW$). This led to a α-value of 1.099. As a result equation 3.35 changed to $P''' = 1.099\ 200\ R'''$. This function was actually used for the power distribution of figure 3.9.

A similar method was used to create a power distribution for the energy deposition on the construction material. MCNP was used for an accurate calculation of the gamma flux and total energy deposition. The gamma flux distribution is depicted in figure 3.10.

Using this distribution, MCNP calculated the total amount of energy deposited by gamma particles on the loop and the inner flood barrier, which is $325W$. Neutron radiation has a similar effect, but the amount of energy deposited due to neutron particles was determined to be around $1W$ for the entire setup. This was considered negligible. The value of β was then varied so that equation 3.39 matches the MCNP value for the deposited energy ($325W$). The resulting power distribution is depicted in figure 3.11.

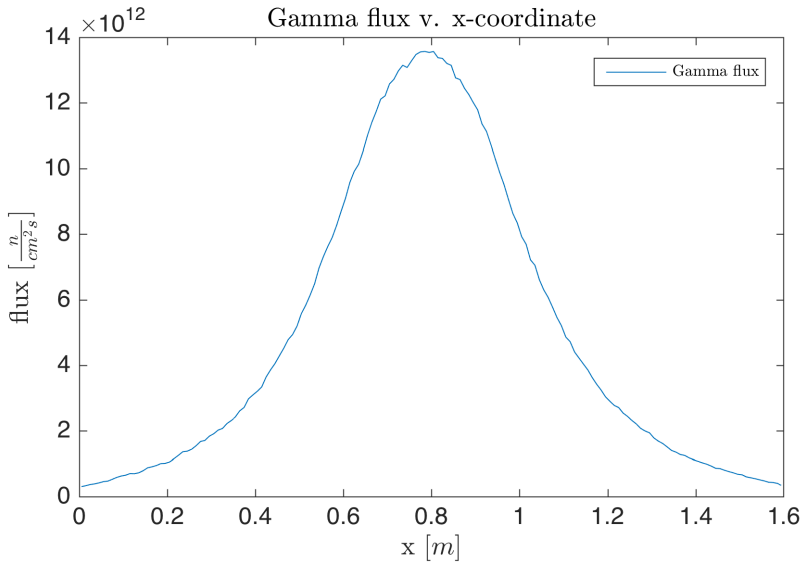

Figure 3.10: Gamma flux distribution

The introduction of the constants α and β is actually useful for another reason. It allows for the adjustment of the heat production in the COMSOL model, which of course effects the maximum temperature inside the loop. But the heat production is also linked to the uranium concentration via the reaction rate 3.34. This means that the effect of the uranium concentration on the maximum temperature can actually be modelled in COMSOL.

3.5. Scale analysis and verification

Due to the loops asymmetric nature, an analytic calculation of the temperature field inside the research loop is not practical. However, the field of transport phenomena does provide some tools to analytically calculate certain properties of the setup. The surface temperature on the interface between the water in the pool and DLDR beam-tube can be determined using dimensionless quantities and Newtons law of cooling (and heating). This law is described by Akker [8] and follows from equation (3.6). It links the heat flux and the temperature difference as follows:

$$\phi_q = hA\Delta T \tag{3.40}$$

- h is the heat transfer coefficient $[W \cdot m^{-2} \cdot K^{-1}]$
- A represents the surface of the object in $[m^2]$.

In cases where both convective and molecular transfer play a role it is often helpful to make use of dimensionless quantities. These numbers are a ratio between different transfer terms, and are useful to characterise a process or problem. The Nusselt number (Nu) for instance characterises heat problems and is defined as the ratio of the total heat transfer and the conductive heat transfer:

$$Nu = \frac{total\ heat\ transfer}{conductive\ heat\ transfer} = \frac{hD}{\lambda} \tag{3.41}$$

This can also be written as:

$$h = Nu\,\frac{\lambda}{D} \tag{3.42}$$

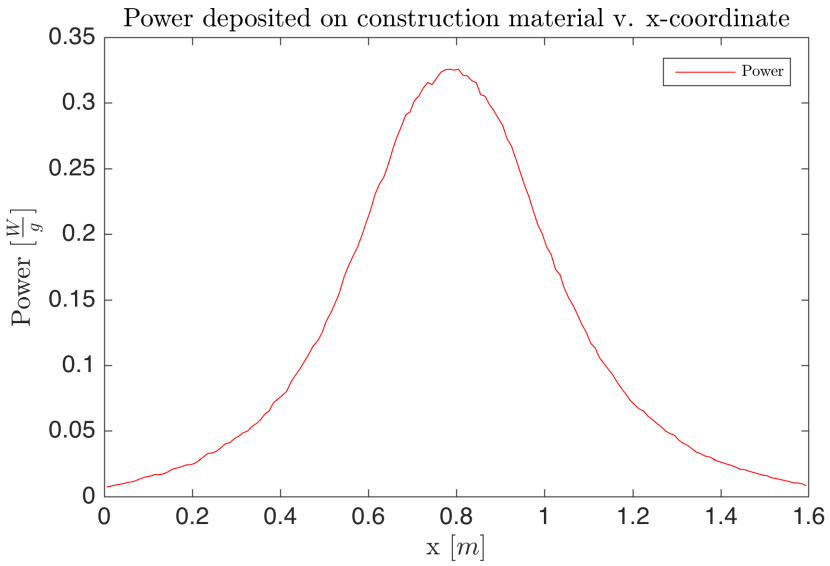

Figure 3.11: Power distribution inside the construction material due to gamma heating

The conductive heat transfer can often be derived for symmetrical problems using equation 3.6. Once Nu is known for a certain geometry, the actual heat transfer can easily be determined. The Nusselt number for a given situation can frequently be found in literature, which makes this kind of quantities particularly useful. The geometry of the DLDR can be described as a horizontal cylinder. The temperature of the beam-tube will be higher than the surrounding water. This will result in a vertical natural convection flow around the cylinder. The Nusselt number for laminar natural convection around a horizontal cylinder according to Boetcher [10] is defined as:

$$Nu = 0.12(Gr\,Pr)^{(1/3)} \tag{3.43}$$

This relation holds for: $10^7 \leq (Gr\,Pr) \leq 10^9$. Where Gr and Pr represent the Grashof number and the Prandtl number. These are defined in Transport Phenomena Data Companion [7] by:

$$Pr = \frac{\nu}{a} \tag{3.44}$$

$$Gr = \frac{D^3 g}{\nu^2}\gamma\Delta T \tag{3.45}$$

- ν is the kinematic viscosity $[m^2 \cdot s^{-1}]$
- a is the thermal diffusion coefficient $[m^2 \cdot s^{-1}]$
- D is the diameter $[m]$
- g is the gravitational constant $[m \cdot s^{-2}]$
- γ is the cubic expansion coefficient $[K^{-1}]$
- ΔT is the temperature difference between the water and the outside surface of the beam-tube $[K]$

A quick calculation of Gr and Pr shows that this relation holds, see appendix A. This also means that the flow around the cylinder is laminar [10]. Combining equations (3.41) - (3.45) results in following relation for Nu:

$$Nu = 0.12\left(\frac{D^3 g}{\nu^2}\gamma Pr\right)^{(1/3)}\Delta T^{(1/3)} \tag{3.46}$$

Section 3.4 determined that the total heat production inside the DLDR beam-tube is $8.195kW$. This study focuses on steady state solutions of the temperature field, so the heat flux ϕ_q exiting the DLDR beam-tube must be equal to the total heat production Q inside. Combining equations 3.40, 3.42, and 3.46 results in:

$$Q = \phi_q = 0.12\frac{\lambda A}{D}\left(\frac{D^3 g}{\nu^2}\gamma Pr\right)^{(1/3)}\Delta T^{(4/3)} \tag{3.47}$$

And rewriting leads to:

$$\Delta T = \left(\frac{D}{0.12\lambda A}Q\right)^{(3/4)}\left(\frac{D^3 g}{\nu^2}\gamma Pr\right)^{-(1/4)} \tag{3.48}$$

Here ΔT is the temperature difference between the bulk of the water and the outside surface of the DLDR beam-tube. Equation 3.48 is an estimation of the surface temperature and will be used to verify the model.

4

Models and simulation in COMSOL

COMSOL Multiphysics is a software package that uses a finite element method to analyse, solve, and simulate various problems in the fields of physics and engineering. This study uses the package in combination with the heat transfer module, which contains modelling tools for the simulation of various transport phenomena.

COMSOL uses a tree like structure that walks the user through a process of defining the different parameters that make up the problem. A model starts out by setting up the physics involved in the problem, followed by defining the geometry. Once the physics and the geometry are set up, boundary conditions can be applied using different nodes. The next sections will cover the different nodes of the tree structure and will go over the choices that have been made.

4.1. Model definition

COMSOL works with so called physics interfaces. Every model starts out by choosing an interface. These interfaces describe certain heat transfer phenomena and can be combined to account for multiple phenomena. In this case, the model needs to account for conduction, convection, and radiation. The physics interface that accounts for these mechanisms is the conjugate heat transfer interface, which has two subinterfaces. One for laminar flow and one for turbulent flow. This study used the laminar flow subinterface. The assumption that the flows inside the loop are laminar needs to be verified.

The setup has different domains and the type of flow has to be verified for every domain. The different domains are defined in figure 4.5

The previous chapter showed that the flow around the beam-tube is laminar. Using dimensionless quantities, the same can be proven for flow in domain 1, inside the loop. Flow through a pipe is laminar if the Reynolds number $Re < 2000$ [8]. Re is defined in the data companion [7] as:

$$Re = \frac{\rho v D}{\eta} \tag{4.1}$$

- $\rho = 1.33\ [g \cdot cm^{-3}]$ is the density
- $v = 2.91 \cdot 10^{-4}\ [m \cdot s^{-1}]$ is the flow velocity
- $D = 44\ [mm]$ is the diameter of the loop

- $\eta = 1.22 \cdot 10^{-3}$ $[Pa \cdot s]$ is the dynamic viscosity of the uranyl solution at $100°C$ [13]

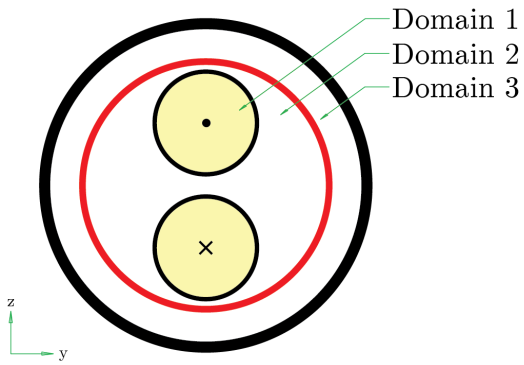

Figure 4.1: Domains inside the setup

Substituting the above parameters in equation 4.1 results in $Re \approx 14.4$, so the flow inside the loop is laminar.

The heat transfer in domain 3 is modelled as natural laminar convection between concentric cylinders as depicted in figure 4.2. Natural convection occurs here due to a temperature difference between the inner and the outer cylinder. This temperature difference causes a temperature gradient in the fluid in domain 3, which results in a density gradient. Under influence of gravity the fluid with a slightly lower density will rise up and the fluid with a higher density will flow down. This leads to a flow pattern in domain 3 depicted in figure 4.2. The assumption of natural laminar convection can be verified using another dimensionless quantity: the Rayleigh number. Ra is defined as:

$$Ra = Gr \cdot Pr = \frac{g\gamma L^3}{\nu a}\Delta T \tag{4.2}$$

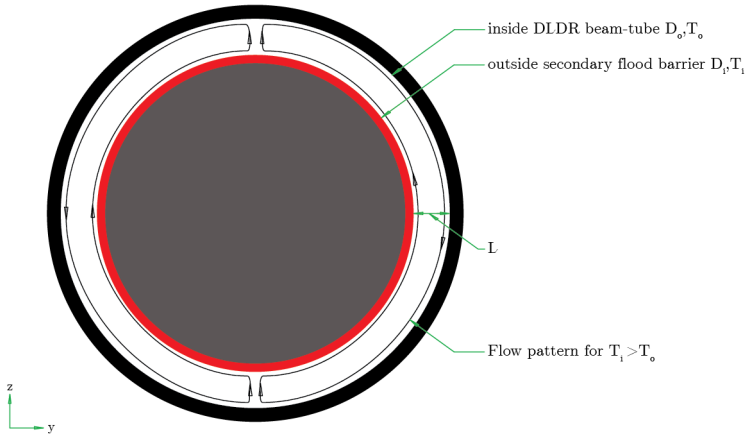

Figure 4.2: Free convection between DLDR and second flood barrier

The Ra number is a dimensionless term associated with natural convection. Natural convection depends on the imbalance of viscosity and buoyancy as well as the fluids ability to dissipate energy. The Ra number is defined as the ratio between the buoyant force and the product of the viscuous drag and the rate of heat diffusion. The low-Rayleigh number limit occurs when the convection boundary layer δ_o exceeds $2L$. This lower limit is known as the critical Rayleigh number Ra_c [10].

$$\delta_o = D_o Ra_{D_o}^{-1/4} > D_o - D_i \tag{4.3}$$

When *Ra* exceeds this value the dominant energy transport mechanism is convection. The onset of turbulent flow occurs at $Ra > 2 \cdot 10^7$ [14] [15] [16]. The thermodynamic properties used for the calculation of *Ra* should be evaluated at the mean temperature.

The model used in this study accounts for both conduction and laminar flows but does not account for turbulence. It is therefore valid for $Ra < 2 \cdot 10^7$ and can be viewed as a worst-case scenario, because turbulent flows would improve heat transfer. So, if heat transfer is sufficient in the laminar case it will be sufficient in general.

The *Ra* number is proportional to the temperature gradient and will therefore reach a maximum when the temperature difference is maximal. This will happen when $T_o = T_{water}$ and $T_i = T_{fuel}$. The water temperature is around $40°C$ and the fuel temperature is limited to $100°C$, which means $\Delta T_{max} = 60°$.

The model compares heat transfer of different heat transfer fluids in domains 2 and 3, so *Ra* needs to be evaluated for every fluid separately in domains 2 and 3.

	$Rayleigh_{max}$
D_2O	$1 \cdot 10^7$
$Helium$	$1.62 \cdot 10^2$

Table 4.1: Maximum *Ra* numbers for fluids in domain 3

The values of Ra_{max} are below the upper limit set in this section. This means that the assumption of laminar flow inside the setup is correct.

The evaluation of domain 2 is more complicated. Due to the non-symmetrical geometry, calculating the *Ra* number for this domain analytically is not possible. Based on the calculations performed for domain 3, this study assumes the natural convective flow in domain 2 to be laminar as well. Once again this can be viewed as the worst-case scenario.

Once the physics has been set up, there are four branches in the tree structure of COMSOL that must be used to assign properties, boundary conditions and production terms.

4.2. Geometry

The geometry branch is used to define the geometry of the problem. This can either be done by importing an existing geometry or by using COMSOLs build-in CAD software. This study uses COMSOLs CAD software to build the setup.

In order to reduce calculation time, only half of the geometry was simulated using a symmetry boundary. The assumption was that the heat production is uniform anywhere inside the loop. In practice however this is not true, as a result of self-shielding the neutron and gamma flux densities will decrease as they pass through the setup. This gradient in the flux between the side facing the core and the opposite side will result in a similar gradient in the heat production. MCNP accounts for the effect of self-shielding. The fluxes used in section 3.4 are the average fluxes inside the loop. These averages are also used for the heat production, which makes this assumption reasonable. Figure 4.3 depicts the used geometry.

The geometry is built using a series of primitives, the specifications of which can be found in the appendix. In order to reduce calculation time even further, the cylinder walls are modelled as a

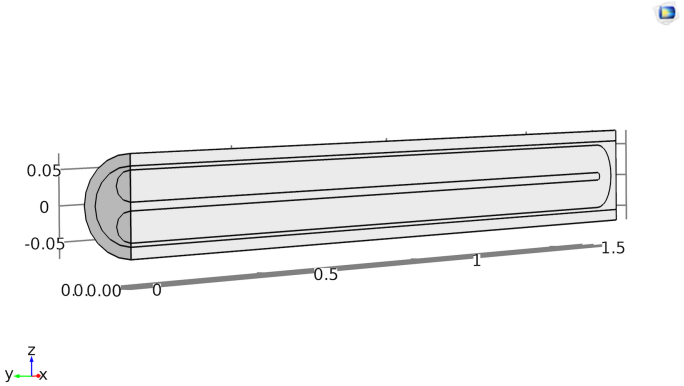

Figure 4.3: Modelled geometry

single boundary. The heat transfer through the walls is modelled using COMSOLs thin layer node. This option defines thickness and thermal properties of a thin thermally conductive material on a boundary. It models the heat transfer through the cylinder wall using a linear relation, which is a good approximation for heat transfer through thin cylinder shells.

4.3. Materials

The materials branch is used to assign materials to different parts of the geometry. The material picked for the loop is Zircaloy, which has a high corrosion resistance. The material used for the inner flood barrier is $AlMg_3$ which is the same material the DLDR is made of.

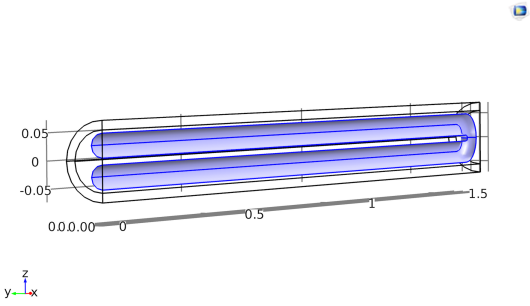

(a) Loop material: Zircaloy

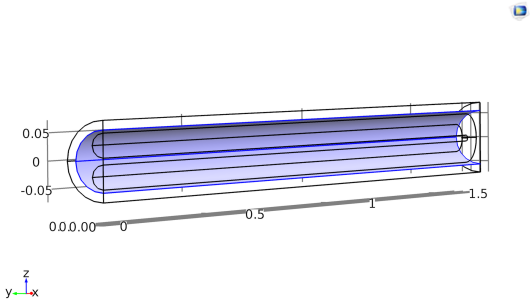

(b) Inner flood barrier material: $AlMg_3$

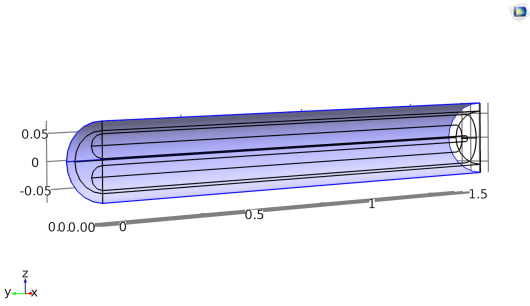

(c) DLDR beam-tube material: $AlMg_3$

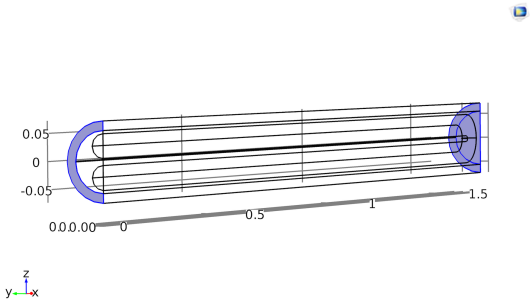

(d) Flange material: $AlMg_3$

Figure 4.4: Used construction materials

Figure 4.4 is an overview of which layer was assigned what material. As stated in chapter 3 COMSOLs extensive library was used for any material properties that were needed. The materials modelled as heat transfer fluid are helium and deuteriumoxide. The COMSOL library does not hold any thermophysical properties of heavy water, but these are similar to the properties of water. So in absence of these properties the properties of normal water were used. Four different combinations of helium and heavy water were simulated.

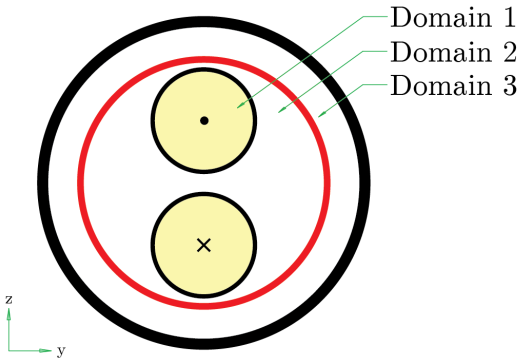

Figure 4.5: Domains inside the setup

Table 4.2 is an overview of the different combinations of heat transfer fluids modelled. As stated earlier in chapter 3 the fuel was modelled using thermophysical properties of water whenever a property of uranyl nitrate was not available.

Combination	Domain 1	Domain 2	Domain 3
1	Fuel	D_2O	D_2O
2	Fuel	D_2O	Helium
3	Fuel	Helium	D_2O
4	Fuel	Helium	Helium

Table 4.2: Modelled combinations of fluids

In order to simulate convection, the density of both helium and heavy water needs to be a function of the temperature. The thermal properties of water in the COMSOL library are temperature dependent, but the properties of helium are not. The density of helium in the property library is therefore overwritten using the ideal gas law.

$$\rho = \frac{ht.pA \cdot M_{He}}{R \cdot T} \tag{4.4}$$

Where $ht.pA$ is the local pressure as defined by COMSOL, M_{He} is the molar mass of helium, R is the universal gas constant, and T the local temperature.

4.4. Heat transfer

The heat transfer branch is used to set initial values, apply boundary conditions, and assign heat production terms. This section will discuss the choices that have been made.

4.4.1. Boundaries

The DLDR wall is modelled as a single boundary (figure 4.6a) as stated in section 4.2. The heat flux node is applied to this boundary, which is used here to model external natural convection in water. The temperature of the water is set to $40°C$.

The boundaries at the mirror plane (figure 4.6b) are modelled using the symmetry node. This node can be used to model symmetric boundaries. It is similar to a thermal insulation condition and it means that there is no thermal flux across the boundary.

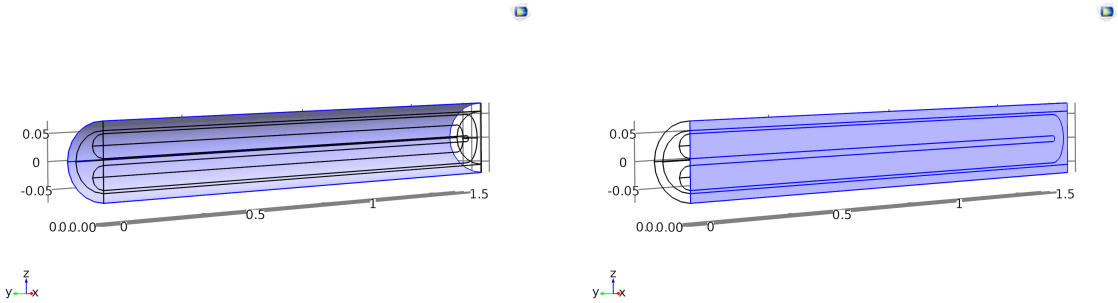

(a) Boundary condition on DLDR: Heat flux

(b) Boundary condition on mirror plane: Symmetry

Figure 4.6: Used boundary conditions

As stated in subsection 3.1.2, the beam-tube is currently closed by two flanges. The DR side of the beam-tube will remain closed by a flange (righthand side in figure 4.7). The tube however does not end behind this flange. It goes on for another couple of meters before it actually ends. At the actual end the DR opening is again closed off with a second flange. The air trapped between this inner and outer flange will act as a thermal insulator. The flange at the DR side is therefore modelled using the thermal insulation node.

The flange at the DL side of the beam-tube will be removed and replaced by a cylinder that acts as an inner flood barrier. Recall however that the Borium shielding present at both the DL and DR side of the beam-tube limits the useable diameter. The shielding closes off the gap between the beam-tube and the inner flood barrier and is modelled as an annulus on the boundary at the end of the DL side. Since this study makes a conservative estimation, the condition applied to this boundary is the thermal insulation node. See figure 4.7a.

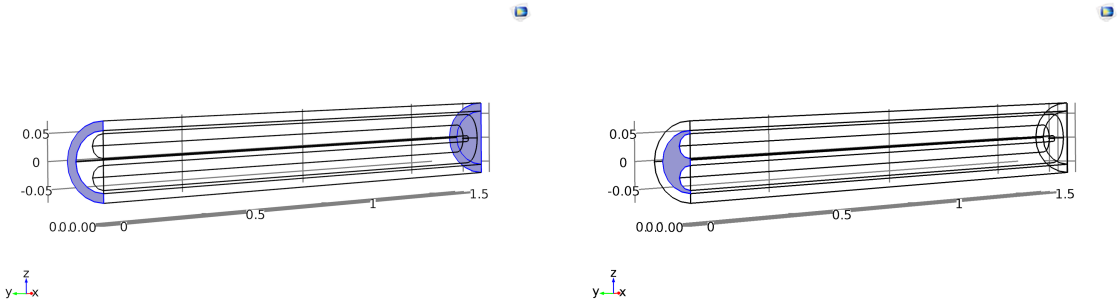

(a) Boundary condition on flanges: thermal insulation

(b) Boundary condition at opening: open boundary

Figure 4.7: Used boundary conditions

The remaining circle on the DL side of the beam-tube is an open boundary and is thus modelled using the open boundary node, see figure 4.7b.

The boundaries at the inlet and outlet, shown in figure 4.8, were modelled using the temperature node and the outflow node. The temperature node models a boundary as having a constant temperature. The salt flow entering domain 1 through this boundary will have this temperature as well. It was estimated that the flow entering the setup would have an average temperature of 30°C, so the temperature node was set to this value.

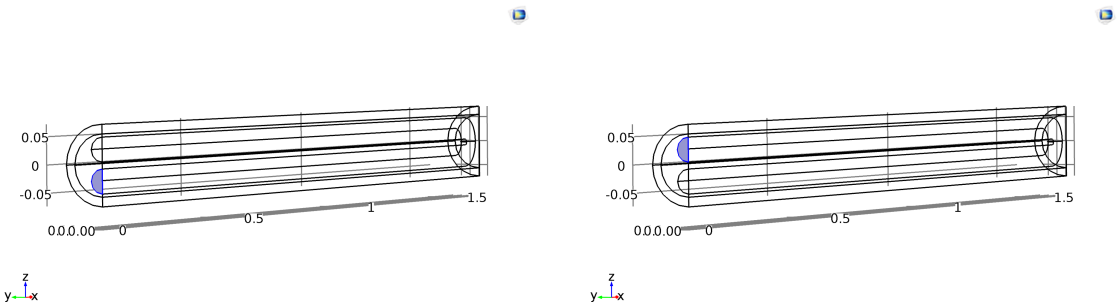

(a) Boundary condition at inlet: temperature

(b) Boundary condition at outlet: outflow

Figure 4.8: Boundary conditions at inlet and outlet

The outflow node is a suitable boundary condition for heat transfer at outlet boundaries. It assumes convection dominated heat transfer. It is a good approximation of the conditions at the outlet of fluid flows.

4.4.2. Heat sources

The heat production inside the loop due to fission is modelled using the power distribution depicted in figure 3.9. The heat source is assigned using the heat source node to the domain shown in figure 4.9.

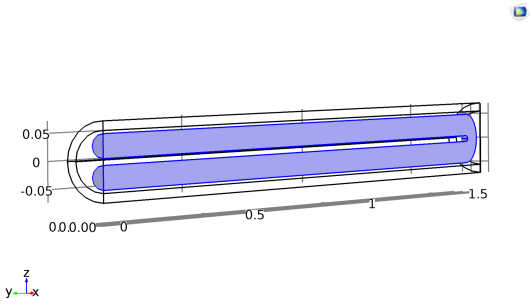

Figure 4.9: Heat source assigned to domain using heat source node

The heat source node allows the user to assign a constant value or a function as a heat source inside a certain domain. In this case the fission power distribution was imported in COMSOL as a function and then assigned to the domain using this node. The function was also assigned a variable α as discussed in subsection 3.4.3. This allows the model to vary the heat production due to fission inside the loop. The gamma heating was modelled using the layer heat source subnode, which is a

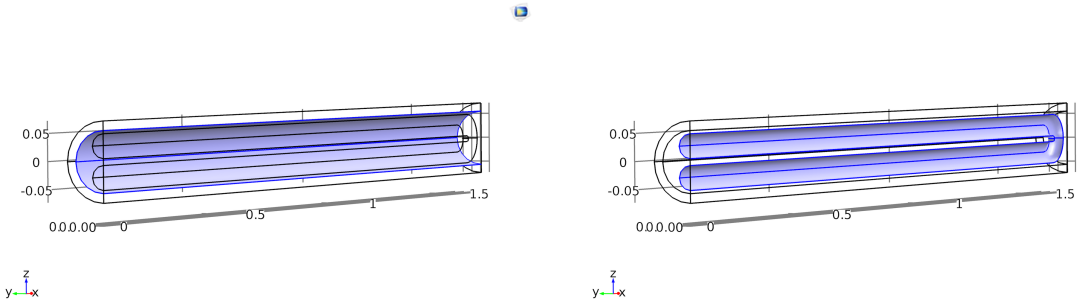

(a) Energy deposited on inner flood barrier

(b) Energy deposited on loop shell

Figure 4.10: Gamma heating sources assigned using the layer heat source subnode

subnode located under the thin layer node. The gamma heating was defined in a similar manner as the fission heating. The gamma power distribution was first imported as a function and afterwards assigned to the thin layers shown in figure 4.10 using the layer heat source subnode. The energy deposited due to gamma heating only dependents on the gamma flux. It has a fixed value and therefore the imported function was not assigned a variable.

4.4.3. Radiation

Heat transfer through radiation is modelled by defining diffuse surfaces and transparent domains. The diffuse surfaces emit radiation as described by equation 3.10, with an emissivity e of 0.2 [17]. This emission coefficient was confirmed to be realistic by the HOR Development.

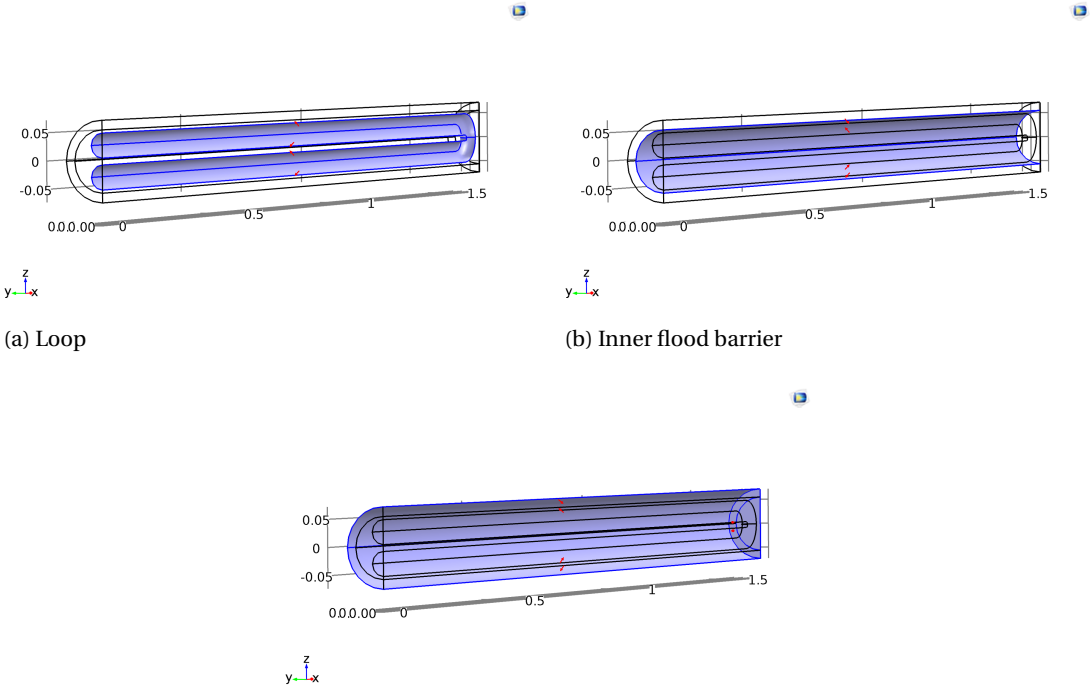

(a) Loop

(b) Inner flood barrier

(c) Beam-tube and DR flange

Figure 4.11: Evaluated directions of radiative fluxes

The direction of this radiation is opacity controlled. The solid materials are defined as opaque and the fluids as transparent by default in COMSOL. The exterior is also defined as transparent. The diffuse surfaces and radiation directions are displayed in figure 4.11

So how does COMSOL evaluate the radiation? For every point on a diffuse surface there are two radiative fluxes. Take for example a point A, which has an outward radiative flux called the radiosity and an inward radiative flux called the irradiation. The irradiation is a result of the local temperature and the radiosity of other points that can "see" point A. These two fluxes need to be balanced to obtain the net radiative flux at point A. COMSOL evaluates the net radiative flux for every point by balancing the radiosity and the irradiation. The net radiative flux is then added to the heat balance.

And lastly, the heat transfer branch also defines the initial temperature of the setup. This has been chosen the be equal to the water temperature, which is $40°C$.

4.5. Laminar flow

The laminar flow branch is used to set the initial values of the flow field and apply boundary conditions to the flow. It is used to calculate the velocity and pressure field of the flow inside the setup in the laminar regime.

4.5.1. Boundaries

The boundaries at the mirror plane are modelled using the symmetry node. This condition has the same effect as the symmetry node used for the mirror plane in the heat transfer branch, meaning the net flux across the boundary is zero.

The boundaries that make up the walls inside and around the setup are modelled using the wall node. This node models the walls using a no-slip condition. This condition prescribes that the velocity at the boundary $v = 0$, ie. the fluid is not moving at the wall. This is justified by reasoning that the fluid particles close to the wall feel an attractive force of the solid particles in the wall, which is called adhesion. It is assumed here that the adhesion force is slightly greater than the force between fluid particles or cohesion. This imbalance results in a zero fluid velocity at the fluid-solid interface.

The inlet and outlet nodes are used to define the inflow and outflow of the fuel. It defines the inlet velocity and the outlet pressure. As stated earlier, a full radiation cycle takes 3 hours. This leads to an inlet velocity of $v_{in} = 2.91 \cdot 10^{-4}\ m \cdots^{-1}$. The outlet pressure is set to atmospheric pressure.

4.5.2. Initial values

There are two initial values that have to be set for all 3 domains, the velocity field and the pressure. The velocity of the fuel at the start of the simulation has been set to zero and the pressure inside the loop to the atmospheric pressure $p_0 = 1.01^5 Pa$.

The initial values of the velocity fields inside domains 2 and 3 have been set zero as well. The initial values of the pressure field inside the domains 2 and 3 have been modelled using a linear relation.

This initial value helps COMSOL converge to a solution and reduces calculation time.

$$p = p_0 - \rho_0 g z \tag{4.5}$$

Finally the last condition applied to the domain 2 and 3 is the volume force node. This node specifies the right hand force term in the Naviers-Stokes equations 3.29 and accounts for the effect of gravity on a domain. The function assigned to this condition is:

$$F = -\rho g \hat{z} \tag{4.6}$$

4.6. Mesh

The used mesh is a physics controlled mesh, with an extra coarse element size setting. A finer mesh setting would lead to a better approximation of the solution, but would also mean a longer run time. The chosen settings are a compromise between accuracy and calculation time. The run time for the calculation of a model using this settings is around 8 hours.

The allowed relative error on all calculations can be set manually in COMSOL. This error was set to 0.0001, which translates to a maximal error in the temperature of around $0.03K$.

5

Results

The model described in chapter 4 was built for different combinations of heat transfer fluids inside domains 2 and 3. These different combinations were described in section 3.2 and can be found in table 5.1.

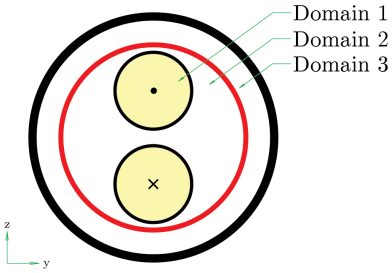

Figure 5.1: Defined domains in the setup

Model	Domain 1	Domain 2	Domain 3
1	Fuel	D_2O	D_2O
2	Fuel	D_2O	Helium
3	Fuel	Helium	D_2O
4	Fuel	Helium	Helium

Table 5.1: Modelled combinations of heat transfer fluids

Chapter 3 showed that the heat production inside the loop due to fission can be adjusted by changing the concentration of uranyl nitrate in the fuel. The variable α was introduced for that purpose to allow COMSOL to change the heat production.

Instead of changing the value of α manually for every simulation, COMSOLs parametric sweep function is used. This parametric sweep runs the model several times and changes the value of the variable α for each simulation. These simulations resulted in steady state solutions of the temperature and flow field inside the setup for every fluid combination and heat production. The steady state solutions to the temperature field can then be used find the maximum temperature inside the loop for each configuration.

The goal of this study is to maintain a safe operating temperature for the research loop. The upper temperature limit has been set to $100°C$. This chapter will go over the different solutions of the temperature field and will compare different configurations. The goal is to find a maximum power production while keeping the temperature under the set limit.

5.1. Model 1: heavy water - heavy water

The configuration with deuteriumoxide in both domain 2 and 3 has the best overall heat transfer. This can be explained by the fact that the thermophysical properties of deuteriumoxide, which are similar to the properties of water, are better for transporting heat than those of helium.

The heat production due to fission was varied from $0W$ to $800W$ with a step size of $200W$, which caused the maximum temperature inside the loop to vary from $107°C$ to $47°C$. The gamma heating was kept constant at $325W$.

$P_{fission}[W]$	$T_{max}[°C]$
800	107.0
600	92.0
400	76.7
200	61.0
0	47.0

Table 5.2: Maximum temperature inside setup for different values of the heat production due to fission

Table 5.2 shows the maximum temperatures inside the setup and the corresponding power production. A power production $P_{fission} = 600W$ would result in a maximum temperature of $92°C$. Figure 5.2a shows the steady state solution to the temperature field inside the setup for $P_{fission} = 600W$.

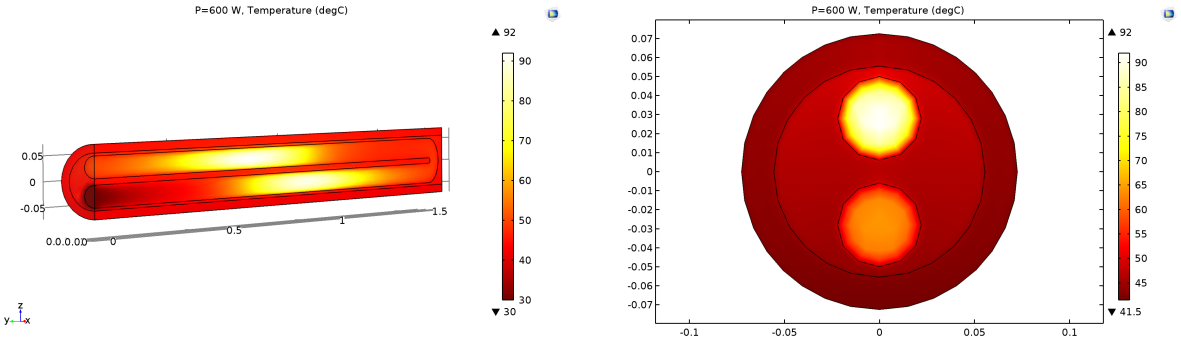

(a) Temperature field inside setup for $P = 600W$

(b) 2D temperature field for $P = 600W$. yz-plane at $x = 0.65m$

Figure 5.2: Temperature field of the model with D_2O in domain 2 and helium in domain 3

The fuel is heated due to the neutron and gamma fluxes as it travels along the x-direction and back through the loop. Because the gamma and neutron fluxes peak at the center of the loop, the maximum temperature also occurs at the center part of the setup. As expected the temperature drops around the U-turn, since the fluxes are nearly zero at that location.

The highest temperature also seems to occur at the center of the loop in the yz-plane 5.2b. This was to be expected since the model does not account for convection inside domain 1, ie. the loop. This might be a shortcoming of the model. In practice the hotter fuel will travel upward inside domain 1 as a result of convection. This effect might improve heat transfer.

In order to get some more insight into the temperature profile, the fuel temperature can also be plotted against the distance the salt travelled. This was done by parameterising the path the fuel travelled and plotting the temperature of the fuel on this path.

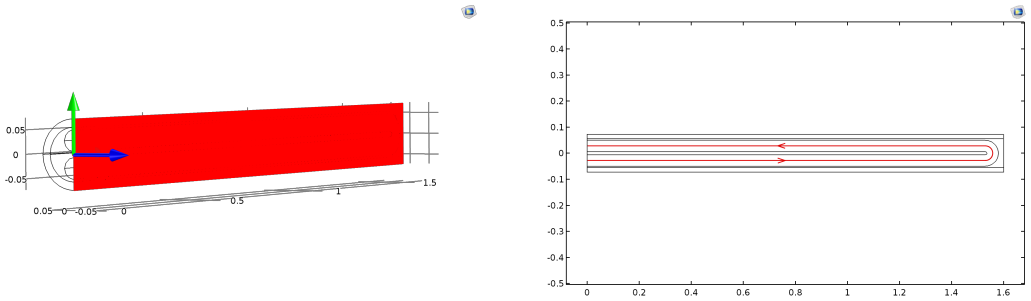

(a) Plane used for parameterisation

(b) Parameterising of path

Figure 5.3: Path travelled by fuel through the loop

Figure 5.4 depicts the temperature as a function of the path shown in figure 5.3b. The different graphs represent core temperatures for different values of the heat production.

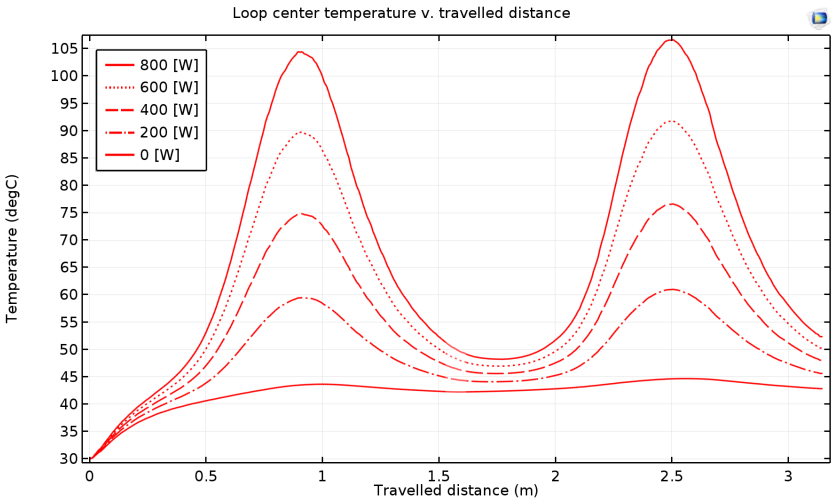

Figure 5.4: Model 1: Temperature loop core v. travelled distance by fuel

The solutions to the temperature field can be partly verified using equation 3.48. The average surface temperature of the beam-tube calculated by comsol can be compared to the temperature calculated using equation 3.48, see appendix A.

$P_{fission}[W]$	$T_{surf,analyti}[°C]$	$T_{surf,comsol}[°C]$
800	43.7	43.0
600	43.2	42.6
400	42.7	42.2
200	42.1	41.7
0	41.5	41.1

Table 5.3: Analytically and numerically calculated surface temperatures of DLDR (note: T for P=0 is elevated because of the gamma heating)

The analytical and numerical calculated temperatures differ less than 2%, so they are in agreement. The slightly higher value of the analytically calculated temperatures can be explained by the fact that equation 3.48 does not account for the inflow and outflow of fuel. The minimal difference between

the two values can be attributed to the very low flow velocity. Increasing the flux would certainly increase the difference.

One last note on the verification: It is based on the total heat production and the properties of the water outside the DLDR. It is therefore independent of materials inside setup and will be valid for all 4 models.

5.2. Model 2: heavy water - helium

The configuration with deuterium oxide in domain 2 and helium in domain 3 is the second model that was simulated. Its heat transfer was found to be less effective than the model with deuterium oxide in both domain 1 and 2. This causes the maximum temperature inside the setup to rise significantly. Table 5.4 shows the maximum temperature for different values of the heat production as a result of fission.

$P_{fission}[W]$	$T_{max}[°C]$
400	125.6
300	109.8
200	93.7
100	77.0
0	61.5

Table 5.4: Maximum temperature inside setup for different values of the heat production due to fission

The helium in domain 3 is identified as a bottleneck for the heat transfer in this model. The presence of a strong temperature gradient in domain 3 and the fact that this is a steady state solution indicate a high heat resistance. This can be seen in figure 5.5b.

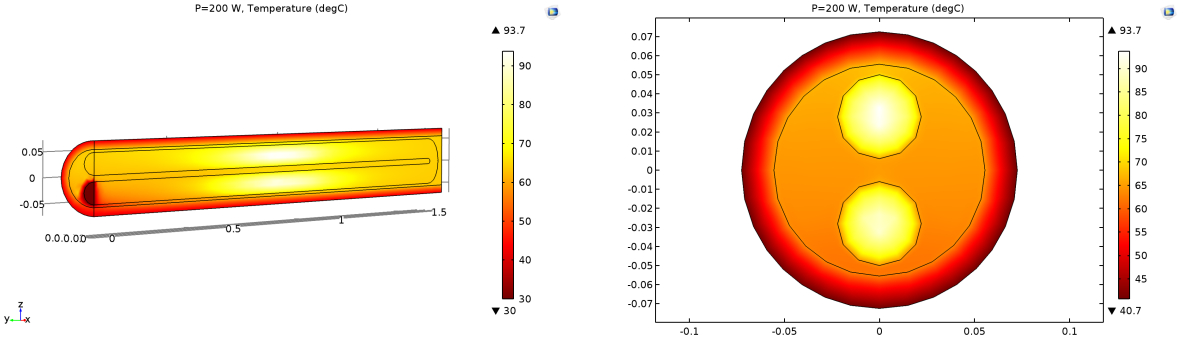

(a) Temperature field for $P = 200$

(b) 2D temperature field for $P = 200$. yz-plane at $x = 0.8m$

Figure 5.5: Temperature field of the model with D_2O in domain 2 and helium in domain 3

As in the previous section the temperature at the center of the loop can also be plotted against the distance travelled by the fuel. This graph can been seen in figure 5.6.

When comparing figure 5.6 to figure 5.4, one of the eye catching differences is the sharp rise in temperature early on in the graph of figure 5.6. This might seem strange because the gamma and neutron fluxes are almost zero at this point.

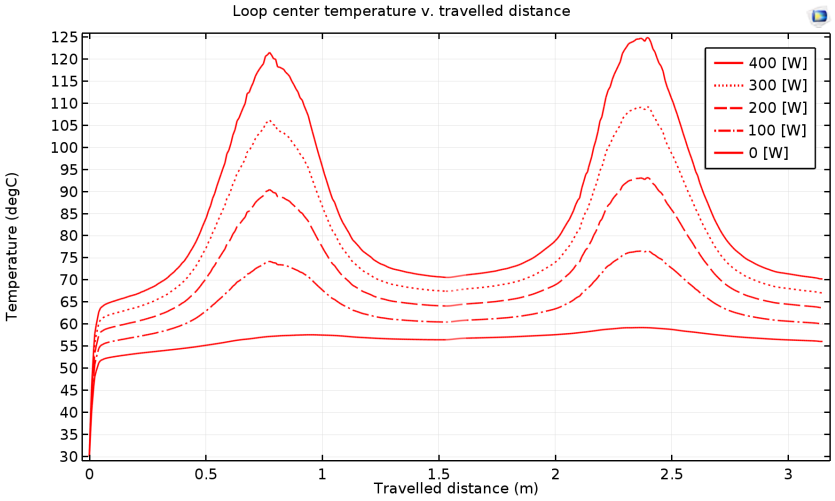

Figure 5.6: Model 2: Temperature loop core v. travelled distance by fuel

The sudden rise is a result of the D_2O present in domain 2 and the helium present in domain 3. Due to the high heat resistance in domain 3 the temperature in domain 2 lies considerably higher than the 40 $°C$ of the surrounding water. At steady state the temperature of the heavy water is almost uniform throughout domain 2. This will cause the fuel to heat up much earlier on in the loop and explains the sharp increase of temperature early on.

5.3. Model 3: helium - heavy water

Model 3 with helium in domain 2 and deuterium oxide in domain 3 showed a slightly worse transfer of heat than model 2. This caused the maximum temperatures inside the setup to be just above the values found for model 2:

$P_{fission}[W]$	$T_{max}[°C]$
240	133.8
180	120.5
120	107.7
60	96.3
0	84.6

Table 5.5: Maximum temperature inside setup for different values of the heat production due to fission

This is caused by the helium that is now located next to the loop. The helium domain is again the bottleneck and it keeps the thermal energy more concentrated inside the loop than it did in model 2. Table 5.5 shows the maximum temperatures for different values of the heat production for model 3.

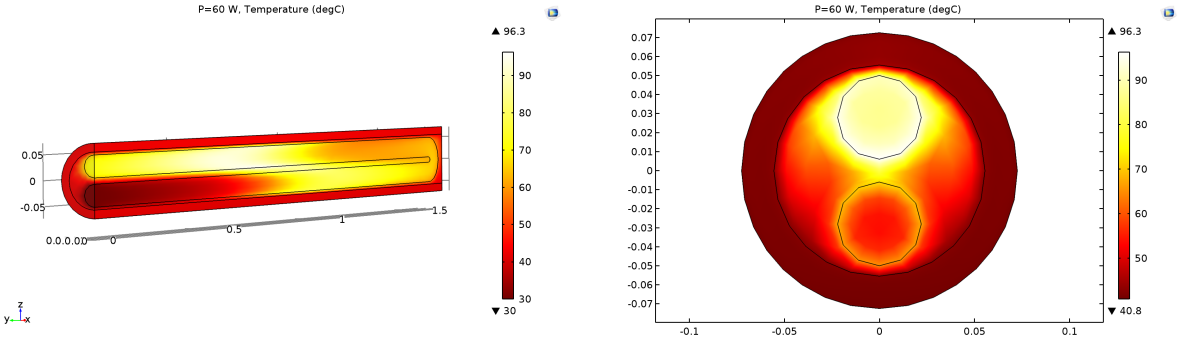

(a) Temperature field for $P = 120$

(b) 2D temperature field for $P = 120$. yz-plane at $x = 0.8m$

Figure 5.7: Temperature field of the model with helium in domain 2 and D_2O in domain 3

Figure 5.7 shows the temperature field of the setup as well as a yz-plane cross section. The cross section clearly shows a strong gradient inside the helium domain which indicates a high heat resistance. Figure 5.8 shows the core temperature as function of the distance travelled by the fuel.

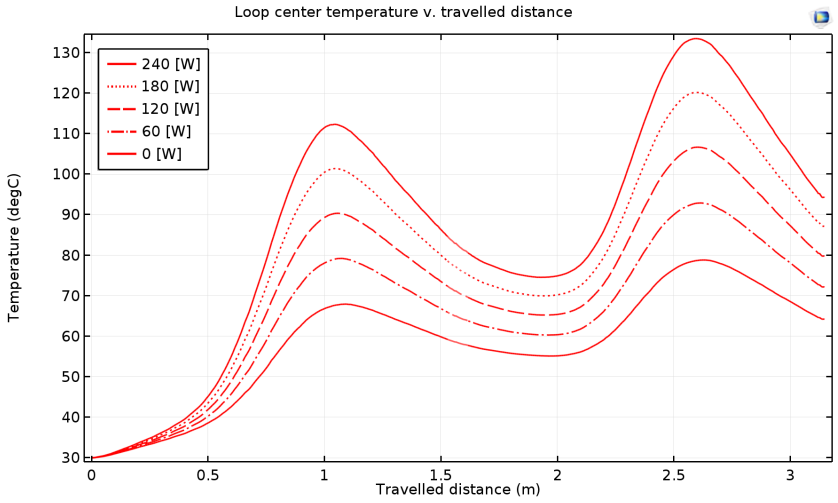

Figure 5.8: Model 3: Temperature loop core v. travelled distance by fuel

Figure 5.8 depicts the temperature of the center of the loop as function of the travelled distance. In comparison to the previous models, the temperature in model 3 decreases less around the U-turn of the loop. This indicates less effective heat transfer than the configurations of model 1 and 2.

5.4. Model 4: helium - helium

Model 4 simulated a setup with helium in both domain 2 and 3. It showed the worst heat transfer of all the models and its maximum temperature was higher than $100°C$ even when the heat production due to fission was set to $0W$. This was to be expected, because in the previous simulations the helium domain proved to be the bottleneck. Table 5.6 shows the maximum temperatures inside the setup.

$P_{fission}[W]$	$T_{max}[^{\circ}C]$
200	178.9
150	163.1
100	148.7
50	134.7
0	120.5

Table 5.6: Maximum temperature inside setup for different values of the heat production due to fission

Figure 5.9 depicts the temperature field inside the setup for a heat production $P_{fission} = 0W$. In this case the only heat source present inside the setup is the gamma heating. Combining the gamma heating with poor heat transfer results in the accumulation of heat inside the construction material. This is reflected in the location of the maximum temperature in the setup. Instead of being located at the center of the upper leg of the U-tube in figure 5.9b, the maximum temperature is reached inside the construction material of the loop.

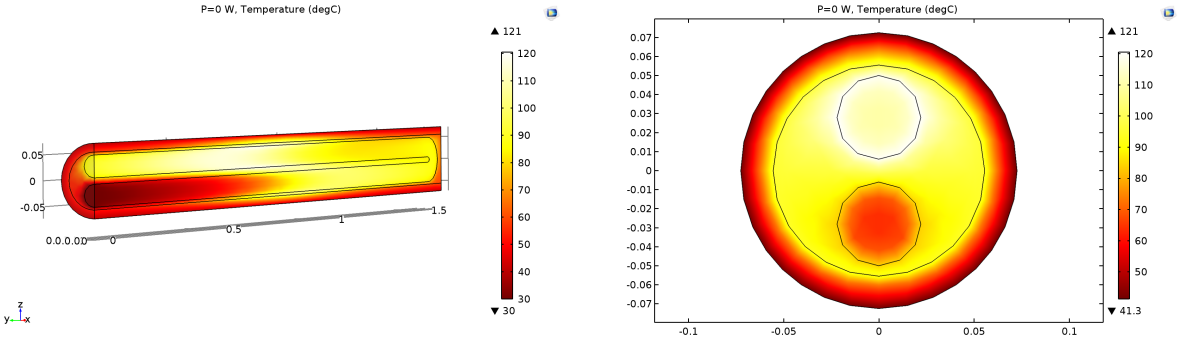

(a) Temperature field for $P = 0$

(b) 2D temperature field for $P = 0$. yz-plane at $x = 0.8m$

Figure 5.9: Temperature field of the model 4 with helium in both domain 2 and 3

Figure 5.10 depicts the temperature of the loop core. Due to the poor heat transfer the fuel cools down less in the midsection of the graph than in the previous models.

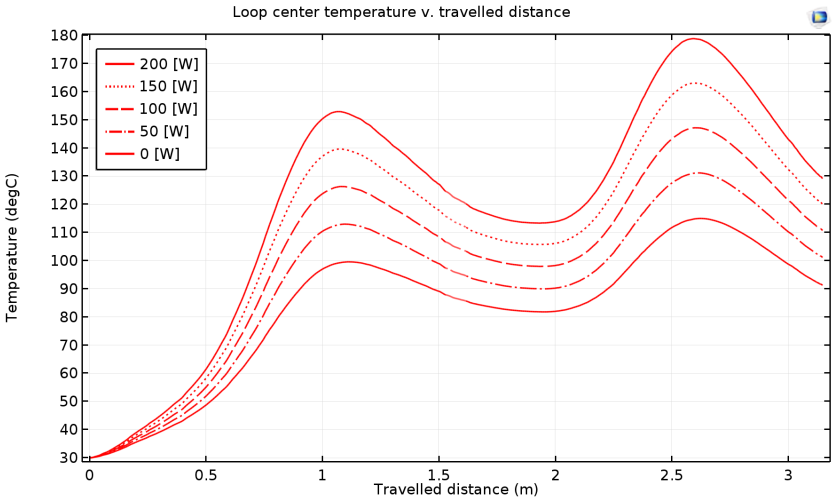

Figure 5.10: Model 3: Temperature loop core v. travelled distance by fuel

5.5. Comparisons

As expected, model 1, with D_2O in domains 2 and 3, shows the most efficient heat transfer. This can be attributed to the better thermophysical properties of deuterium oxide. Model 2 was second best, model 3 third, and model 4 last.

The maximum temperatures of tables 5.2 - 5.6 are plotted in the graph of figure 5.11 and are fitted using a linear fit to estimate the maximum heat production that keeps the temperature below $100°C$.

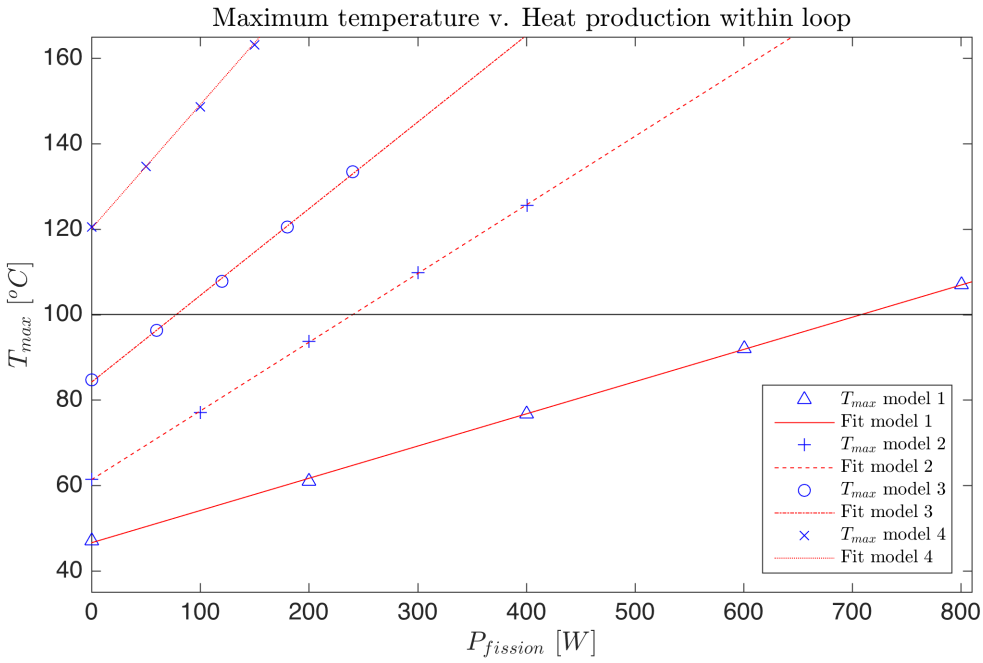

Figure 5.11: Comparison of maximum temperatures of different models

Table 5.7 is an overview of the intersections of the fits of figure 5.11 with $T_{max} = 100°C$. It shows that the maximum allowed heat production due to fission for model 1 is $700W$. This excludes the power produced by gamma heating. The total power production inside the setup would amount to $1025W$.

Model	Domain 1	Domain 2	Domain 3	P_{gamma} [W]	$P_{fission}$ [W] @ 100°C
1	Fuel	D_2O	D_2O	325	700
2	Fuel	D_2O	Helium	325	240
3	Fuel	Helium	D_2O	325	70
4	Fuel	Helium	Helium	325	N/A

Table 5.7: Maximum allowed $P_{fission}$ for $T < 100°C$

The Mo-99 yield of the setup increases for higher concentrations of the uranyl nitrate solution. Section 3.4 showed that the uranium concentration is proportional to power production inside the setup. In order to maximise the yield and maintain a safe operating temperature, the setup should have an optimal heat transfer. Table 5.7 shows that this is the case for a setup with deuterium oxide in domain 2 and 3, and that the maximum allowed heat production for this configuration is $P_{fission} = 700W$.

5.6. Notes on the concentration of uranium

Section 3.4 showed that the heat production is directly proportional to the concentration:

$$P_{fission} \propto c \tag{5.1}$$

By assuming that this relation is linear, it is possible to make a rough estimation of the concentration of uranium in the fuel that corresponds to the values of the heat production in table 5.7:

$$P_{fission} = nc \tag{5.2}$$

Where n is a constant. The MCNP calculations showed that a uranium concentration of $c = 310 g\ U\ L^{-1}$, with an enrichment of $\varepsilon = 0.2$, would lead to a heat production of $P_{fission} = 7.87 kW$. This results in a n-value of $n = 25.3871$, which is used to estimate the upper uranium concentration limits for each model.

Model	P_{gamma} $[W]$	$P_{fission}$ $[W]$ @ $100°C$	c $[g\ U\ L^{-1}]$
MCNP	325	7870	310
1	325	700	27.6
2	325	240	9.5
3	325	70	2.8
4	325	N/A	N/A

Table 5.8: Maximum allowed $P_{fission}$ for $T < 100°C$

Table 5.8 shows that, for model 1, the maximum concentration of uranium that keeps the temperature under $100°C$ is $c = 27.6 g\ U\ L^{-1}$. The enrichment of these solutions is 0.2.

Alternatively, the level of enrichment may be lowered to achieve the same power production inside the loop instead of lowering the concentration. The advantage of this method is that it might be safer to work with lower levels of enrichment. The downside is that a higher concentration of uranyl nitrate leads to a higher acidity of the solution.

Note that these calculations are very rough and may be oversimplified.

6

Conclusions and discussion

This research studies the suggested design for a reactor loop aimed at the efficient production of molybdenum-99 inside the HOR. The goal of this study is to determine operating conditions which would result in a safe operating temperature for this loop. The maximum operating temperature considered safe was decided upon beforehand and was set to $100°C$.

In order to determine the maximum temperature, this study investigated the overall heat transfer of the suggested design by modelling the setup and simulating the fluid dynamics in COMSOL Multiphysics. The setup was modelled and simulated for different configurations. The results indicate that the heat transfer of the loop will limit the production capacity of the setup, and that, in order to maximise the yield, the heat transfer will have to be optimised. Within the framework of this research, the efficiency of the overall heat transfer was dominated by the choice of heat transfer fluid. This study achieved the most efficient heat transfer when using deuterium oxide.

Different materials and configurations where simulated in COMSOL. The conclusions are divided over different categories, namely construction materials, heat transfer fluids, heat production, and uranium concentration.

6.1. Geometry

The initial design had to be altered to accommodate a necessary safety measure. The DLDR beam-tube has two flanges at both ends which function as a secondary flood barrier. This function needs to be maintained during and after installation of the research loop. This is achieved by replacing one of the flanges by a cylinder, with one side closed off. The cylinder will be placed inside the DLDR and contains the research loop. This ensures that if the DLDR would leak, the reactor hall would not be flooded. And similarly, if the loop leaks, the fuel will not come in contact with the DLDR.

Different construction materials were considered for the setup. The DLDR beam-tube is made from an aluminum magnesium alloy, $AlMg_3$, which is an alloy with excellent construction properties. Due to its low cross section it is almost completely transparent to neutrons. The alloy was considered for use inside the setup as well, but discarded due to its low corrosion resistance.

Uranyl nitrate solutions have a high acidity and can reach a pH as low as 0.5, depending on the concentration. Therefore a construction material needs to have a high corrosion resistance. Zircaloy

is an alloy widely used in nuclear industry. It has a high corrosion resistance and a low neutron cross section, making it an excellent choice for both the loop and the secondary flood barrier.

6.2. Heat transfer fluids

The heat transfer fluids that were considered are deuterium oxide and helium. Deuterium oxide showed to be far superior to helium when it comes to the overall heat transfer of the setup. A configuration with D_2O in both domain 2 and 3, would allow for a heat production of $1025kW$ and would thus allow for a higher yield of Mo-99.

Deuterium oxide was chosen over regular water because it has a lower neutron cross section, and thus has a smaller effect on the neutron flux inside the loop. It is preferable to have a neutron flux that is as high as possible. A higher neutron flux allows for a lower uranyl nitrate concentration while maintaining the same reaction rate.

Helium allows for an even higher neutron flux, but its poor thermophysical properties cause the heat transfer to be insufficient for this setup.

6.3. Heat production

The heat production inside the setup was calculated in MCNP and can be split up into two parts, gamma heating and fission heating. The gamma heating is a result of the deposition of energy onto the construction material by the gamma flux. It was calculated in MCNP that the deposited heat on the construction material adds up to $325W$.

The heat production due to fission is a result of the neutron flux inside the setup. The neutron flux and the heat production were both calculated in MCNP and used to produce a power distribution. The power distribution and the gamma heating were then used to determine the temperature field inside the setup for different configurations.

As stated in the previous section, the most efficient heat transfer was achieved using deuterium oxide as heat transfer fluid. Using this configuration the highest heat production that kept the maximum temperate below $100°C$ was $P_{total} = P_{fission} + P_{gamma} = 1025W$.

6.4. Uranium concentration

The uranium concentration corresponding to the heat production of $1025W$ is roughly estimated to be $27.6g\ U\ L^{-1}$. This concentration has a level of enrichment of 0.2. Alternatively the level of enrichment may be lowered in favor of a higher concentration. A lower level of enrichment is favorable because it is safer and easier to work with, the drawback is that a higher concentration of uranyl nitrate would mean a higher acidity. The higher acidity makes the solution more corrosive.

6.5. Discussion

This research has a couple of considerations and assumptions. First of all the heat production inside the fuel was considered to be only dependent on the x-coordinate. This is not true in practice. The

U-235 will react with the neutrons during its stay in the loop which will result in a lower reaction rate as time passes and thus results in a lower heat production. The heat production will also diminish along the y-coordinate (increasing distance from the reactor core). The neutron flux will also be lower for greater distance from the core, partly because the flux diverges and partly because of the self-shielding effect of the setup.

Furthermore, natural convection was not simulated inside the fuel flow in domain 1. The heat production inside the loop causes the fuel to circulate in the yz-plane perpendicular to the flow direction. This natural convection would most likely improve heat transfer.

And lastly, the MCNP calculations for the neutron and gamma fluxes were only performed using the helium inside domains 2 and 3. These fluxes were used for the power distributions of all four models. Since the presence of D_2O inside the setup would adversely effect the neutron flux, the heat productions for model 1, 2, and 3 are overestimations.

All the assumptions that were made in this study were made using the worst-case scenario.

6.6. Future research

Suggestions for future research include an integral research of both heat transfer and Mo-99 production. This can be achieved by combining both MCNP and COMSOL calculations. This study identified the heat transfer as bottle neck for the production capacity. The implications of this bottle neck for the Mo-99 yield should be further investigated.

A model that combines MCNP and COMSOL would allow for a more accurate description of the heat production, heat transfer, and production capacity. This new model could also account for forced convective cooling in domains 2 and 3, which have not been incorporated in this research. Convective cooling would result in better heat transfer and thus lead to a higher yield.

Other research could include a study of the effects of the acidity of the fuel on the production process and of the corrosive effects of the fuel on the construction materials.

Bibliography

[1] K. Elgin - A study of the feasibility of 99Mo production inside the TU Delft Hoger Onderwijs Reactor - 2014

[2] IAEA - Production and Supply of Molybdenum-99 - 2010

[3] M.V. Huisman - Medical Isotope Production Reactor - 2013

[4] P.A. Schweitzer - Corrosion Resistance Tables: Part D - rev. 5th ed. - 2004

[5] R.H. Fulmer, D.P. Stricos, T.F. Ruane - Neutron Absorption Cross Sections for Zirconium-94 and Zirconium-96 - 1971

[6] S.F. Mughabghab - Atlas of Neutron Resonances - 5th ed. - 2006

[7] L.P.B.M. Janssen, M.M.C.G. Warmoeskerken - Transport phenomena data companion - 3rd ed. - 2006

[8] H.E.A. van den Akker, R.F. Mudde - Fysische transportverschijnselen - 3rd ed. - 2008

[9] R.B. Bird, W.E. Stewart, E.N. Lightfoot - Transport phenomena - rev. 2nd ed. - 2007

[10] S. K. S. Boetcher - Natural Convection Heat Transfer From Horizontal Cylinders - 1st ed. - 2014

[11] J.J. Duderstadt, L.J. Hamilton - Nuclear reactor analysis - 1st ed. - 1976

[12] T. Delorme - Meetrapport gamma-opwarming HOR-O - 1997

[13] E.O. Krahn, A.S. Hebden, G.F. Vandegrift, Pei-Lun C., Nien-Hwa L.W. - Mechanical Stability Study - 2010

[14] T.H. Kuehn - Natural Convection Heat Transfer from a Horizontal Circular Cylinder to a Surrounding Cylindrical Enclosure - 1976

[15] A. Bejan - Convection heat transfer - 4th ed. - 2013

[16] A. Faghri, Y. Zhang, J. Howell - Advanced Heat and Mass Transfer - 1st ed. - 2010

[17] E.V. Murphy, F. Havelock - Emissivity of zirconium alloys in air in the temperature range 100-400 C - 1976

Nomenclature

Elements

$Mo-99$	Molybdenum-99
$Tc-99m$	Technetium-99m
U	Uranium
$U-235$	Uranium-235, uranium isotope with mass number 235. It is fissionable by thermal neutrons
$U-238$	Uranium-238, uranium isotope with mass number 283. It is not fissionable by thermal neutrons
O	Oxide
N	Nitrogen

Abbreviations

PTC	Particle Treatment Center
RID	Reactor Instituut Delft
HOR	Hoger Onderwijs Reactor
LEU	Low-enriched uranium, meaning an uranium-235 percentage < 20 %
HEU	High-enriched uranium, meaning an uranium-235 percentage ≥ 20 %
MTR	Material testing reactor

List of symbols

a	Thermal diffusion coefficient
A	Surface
c	Concentration
c_p	Heat capacity at constant pressure
d	Diameter
D	Diameter
$\mathbb{D}$	Diffusion constant
e	Emission coefficient
E	Energy
F	Force
g	Gravitational acceleration
h	Heat transfer coefficient
k_B	Boltzmann constant
m	Mass
M	Molar mass
n	Amount
N	Amount
N_a	Avogadro constant
p	Pressure

p	Momentum
P	Power
Q	Heat production per volume
R	radius
t	Time
T	Temperature
U	Overal heat transfer coefficient
v	Velocity
V	Volume
α	Fission power fraction
β	γ-radiation power fraction
γ	γ-radiation, radiation in the electromagnetic spectrum
γ	Expansion coefficient
ε	Level of enrichment, ie. the fraction of U-235 present in uranium.
η	Dynamic viscosity
ϕ	Flux
ϕ'	Flux per unit distance
ϕ''	Flux per unit area
ϕ'''	Flux per unit volume
λ	Heat conduction coefficient
μ	Dynamic viscosity
ν	Kinematic viscosity
ρ	Density
σ	Stefan-Boltzmann constant
σ	Microscopic cross section

Dimensionless quantities

Gr	Grashof number
Nu	Nusselt number
Pr	Prandtl numbner
Ra	Rayleigh number
Re	Reynolds number

Appendices

A

Verification and validation

The values in table 5.3 where calculated using equation 3.48:

$$\Delta T = \left(\frac{D}{0.12\lambda A}Q\right)^{(3/4)}\left(\frac{D^3 g}{\nu^2}\gamma Pr\right)^{-(1/4)} \tag{A.1}$$

Where:

- D is the diameter
- λ is the thermal conductivity coefficient
- A is the surface area
- Q is the total volumetric heat production (neutron + gamma heating)
- g is the gravitational constant
- ν is the kinematic viscosity
- γ is the cubic expansion coefficient
- Pr is the Prandtl number
- $\Delta T = T_{surface} - T_\infty$ is the temperature difference between the water and the outside surface of the beam-tube

The values used for the calculation of ΔT were taken from the Data Companion. The temperature difference was expected to be $20°C$. The temperature of the water is around $40°C$. The values of the variables were evaluated at the average temperature of $50°C$.

- $D = 0.15$
- $\lambda = 0.641$
- $A = 1.6 \cdot \pi \cdot D = 0.7540$
- $Q = 1125, 925, 725, 525, 325$
- $g = 9.81$
- $\nu = 0.658 \cdot 10^{-6}$
- $\gamma = 0.385 \cdot 10^{-3}$
- $Pr = 4.34$

Calculation example of $T_{surface}$ for $Q = 1125$:

$$\left(\frac{0.15}{0.12 \cdot 0.641 \cdot 0.7540} \cdot 1125\right)^{(3/4)}\left(\frac{0.15^3 \cdot 9.81}{(0.658 \cdot 10^{-6})^2} \cdot 0.385 \cdot 10^{-3} \cdot 4.34\right)^{-(1/4)} + T_\infty = 43.7°C \tag{A.2}$$

A.1. Validation

Equation 3.48 is valid on the interval $10^7 \leq (Gr \cdot Pr) \leq 10^9$. The Grashof and Prandtl numbers are defined in the Transport Phenomena Data Companion as:

$$Pr = \frac{\nu}{a} \tag{A.3}$$

$$Gr = \frac{D^3 g}{\nu^2}\gamma\Delta T \tag{A.4}$$

Where:

- ν is the kinematic viscosity
- a is the thermal diffusion coefficient
- D is the diameter
- g is the gravitational constant
- γ is the cubic expansion coefficient
- ΔT is the temperature difference between the water and the outside surface of the beam-tube

The temperature difference between the water and the outside surface of the DLDR beam-tube is around $5°C$. The variables used for the calculation of Gr and Pr were evaluated at the mean temperature of $42.5°C$:

- $\nu = 0.579 \cdot 10^{-6}$
- $a = 0.152 \cdot 10^{-6}$
- $D = 0.15$ is the diameter
- $g = 9.81$ is the gravitational constant
- $\gamma = 0.403 \cdot 10^{-3}$ is the cubic expansion coefficient

Running these numbers results in a Ra number of:

$$Ra = Gr \cdot Pr = \frac{0.15^3 \cdot 9.81}{(0.579 \cdot 10^{-6})^2} \cdot 0.403 \cdot 10^{-3} \cdot 5 \cdot 4.15 = 8 \cdot 10^8 \tag{A.5}$$

A Ra number this high indicates the onset of turbulent flow, but it is still within the defined interval of validity. Therefore equation 3.48 can be used.

B

Flux values

The table below shows the average flux values in domain 1 that were used to create the power and flux distributions of figures 3.8 - 3.11. The power distributions were used to define the heat sources in the COMSOL model.

x [m]	thermal [$n\ cm^{-2}\ s^{-1}$]	epi [$n\ cm^{-2}\ s^{-1}$]	fast [$n\ cm^{-2}\ s^{-1}$]	gamma [$n\ cm^{-2}\ s^{-1}$]
0.005	8.37E+09	2.10E+09	1.83E+09	3.06E+11
0.015	1.27E+10	2.46E+09	4.85E+09	3.35E+11
0.025	1.77E+10	3.50E+09	7.55E+09	3.69E+11
0.035	1.89E+10	3.13E+09	8.52E+09	3.90E+11
0.045	2.29E+10	3.77E+09	9.95E+09	4.21E+11
0.055	2.49E+10	5.11E+09	1.04E+10	4.58E+11
0.065	3.02E+10	7.42E+09	1.34E+10	4.74E+11
0.075	3.25E+10	7.06E+09	1.41E+10	5.30E+11
0.085	3.38E+10	7.06E+09	1.37E+10	5.87E+11
0.095	4.08E+10	8.41E+09	1.46E+10	6.29E+11
0.105	4.40E+10	1.08E+10	1.83E+10	6.54E+11
0.115	4.94E+10	9.46E+09	2.33E+10	7.03E+11
0.125	5.33E+10	1.07E+10	2.04E+10	6.99E+11
0.135	6.21E+10	1.03E+10	2.26E+10	7.28E+11
0.145	6.41E+10	1.31E+10	2.54E+10	7.92E+11
0.155	6.46E+10	1.78E+10	2.84E+10	8.80E+11
0.165	7.55E+10	1.69E+10	3.04E+10	9.10E+11
0.175	7.71E+10	1.69E+10	3.25E+10	9.50E+11
0.185	8.00E+10	2.25E+10	4.00E+10	1.01E+12
0.195	8.47E+10	2.29E+10	3.91E+10	1.01E+12
0.205	8.67E+10	2.64E+10	3.94E+10	1.06E+12
0.215	1.00E+11	2.43E+10	4.16E+10	1.15E+12
0.225	1.12E+11	2.66E+10	4.67E+10	1.25E+12
0.235	1.20E+11	2.84E+10	5.31E+10	1.36E+12
0.245	1.33E+11	3.12E+10	5.89E+10	1.37E+12
0.255	1.43E+11	3.47E+10	5.74E+10	1.43E+12
0.265	1.59E+11	3.80E+10	6.56E+10	1.54E+12

0.275	1.65E+11	4.18E+10	7.35E+10	1.67E+12
0.285	1.84E+11	4.85E+10	7.54E+10	1.70E+12
0.295	2.01E+11	4.97E+10	9.54E+10	1.83E+12
0.305	2.28E+11	5.71E+10	9.62E+10	1.91E+12
0.315	2.38E+11	6.28E+10	1.09E+11	2.02E+12
0.325	2.48E+11	5.98E+10	1.22E+11	2.07E+12
0.335	2.74E+11	6.45E+10	1.20E+11	2.22E+12
0.345	3.07E+11	6.44E+10	1.34E+11	2.31E+12
0.355	3.45E+11	6.45E+10	1.50E+11	2.42E+12
0.365	3.60E+11	8.08E+10	1.56E+11	2.60E+12
0.375	3.73E+11	8.56E+10	1.76E+11	2.71E+12
0.385	4.27E+11	9.73E+10	1.86E+11	2.97E+12
0.395	4.60E+11	9.60E+10	2.05E+11	3.09E+12
0.405	5.01E+11	1.21E+11	2.28E+11	3.20E+12
0.415	5.35E+11	1.29E+11	2.46E+11	3.34E+12
0.425	6.01E+11	1.44E+11	2.76E+11	3.64E+12
0.435	6.63E+11	1.54E+11	2.94E+11	3.86E+12
0.445	7.07E+11	1.66E+11	3.22E+11	4.05E+12
0.455	7.68E+11	1.82E+11	3.61E+11	4.28E+12
0.465	8.40E+11	1.97E+11	3.78E+11	4.52E+12
0.475	9.18E+11	2.14E+11	4.22E+11	4.78E+12
0.485	1.03E+12	2.39E+11	4.53E+11	4.94E+12
0.495	1.11E+12	2.58E+11	4.80E+11	5.19E+12
0.505	1.18E+12	3.00E+11	5.24E+11	5.58E+12
0.515	1.28E+12	3.12E+11	5.70E+11	5.84E+12
0.525	1.38E+12	3.46E+11	6.06E+11	6.14E+12
0.535	1.52E+12	3.87E+11	6.56E+11	6.49E+12
0.545	1.61E+12	4.02E+11	7.05E+11	6.97E+12
0.555	1.74E+12	4.50E+11	7.57E+11	7.32E+12
0.565	1.87E+12	4.61E+11	7.87E+11	7.63E+12
0.575	1.94E+12	4.78E+11	8.24E+11	7.90E+12
0.585	2.09E+12	5.14E+11	8.99E+11	8.27E+12
0.595	2.19E+12	5.51E+11	9.79E+11	8.69E+12
0.605	2.30E+12	5.98E+11	1.02E+12	9.09E+12
0.615	2.42E+12	6.30E+11	1.03E+12	9.58E+12
0.625	2.55E+12	6.83E+11	1.12E+12	9.92E+12
0.635	2.66E+12	6.98E+11	1.23E+12	1.01E+13
0.645	2.76E+12	7.33E+11	1.26E+12	1.05E+13
0.655	2.85E+12	7.86E+11	1.30E+12	1.10E+13
0.665	2.97E+12	8.44E+11	1.36E+12	1.14E+13
0.675	3.07E+12	8.60E+11	1.40E+12	1.17E+13
0.685	3.19E+12	8.97E+11	1.44E+12	1.21E+13
0.695	3.25E+12	9.13E+11	1.50E+12	1.22E+13
0.705	3.32E+12	9.49E+11	1.54E+12	1.26E+13
0.715	3.45E+12	9.71E+11	1.54E+12	1.27E+13
0.725	3.52E+12	1.03E+12	1.60E+12	1.30E+13
0.735	3.52E+12	1.05E+12	1.65E+12	1.31E+13

0.745	3.58E+12	1.05E+12	1.67E+12	1.31E+13
0.755	3.57E+12	1.08E+12	1.66E+12	1.33E+13
0.765	3.66E+12	1.09E+12	1.69E+12	1.35E+13
0.775	3.71E+12	1.10E+12	1.74E+12	1.36E+13
0.785	3.70E+12	1.13E+12	1.69E+12	1.36E+13
0.795	3.68E+12	1.13E+12	1.72E+12	1.35E+13
0.805	3.65E+12	1.12E+12	1.72E+12	1.36E+13
0.815	3.64E+12	1.10E+12	1.74E+12	1.34E+13
0.825	3.63E+12	1.07E+12	1.71E+12	1.34E+13
0.835	3.57E+12	1.07E+12	1.67E+12	1.32E+13
0.845	3.56E+12	1.03E+12	1.67E+12	1.31E+13
0.855	3.49E+12	1.01E+12	1.64E+12	1.28E+13
0.865	3.45E+12	9.84E+11	1.61E+12	1.27E+13
0.875	3.33E+12	9.63E+11	1.51E+12	1.24E+13
0.885	3.25E+12	9.06E+11	1.52E+12	1.23E+13
0.895	3.23E+12	9.19E+11	1.45E+12	1.20E+13
0.905	3.08E+12	8.96E+11	1.39E+12	1.18E+13
0.915	2.94E+12	8.57E+11	1.33E+12	1.14E+13
0.925	2.81E+12	8.12E+11	1.28E+12	1.11E+13
0.935	2.73E+12	7.54E+11	1.24E+12	1.07E+13
0.945	2.58E+12	6.97E+11	1.19E+12	1.03E+13
0.955	2.41E+12	6.65E+11	1.08E+12	9.88E+12
0.965	2.25E+12	6.32E+11	1.01E+12	9.51E+12
0.975	2.15E+12	5.81E+11	9.38E+11	9.06E+12
0.985	2.00E+12	5.38E+11	9.04E+11	8.63E+12
0.995	1.85E+12	4.86E+11	7.94E+11	8.34E+12
1.005	1.72E+12	4.42E+11	7.63E+11	7.92E+12
1.015	1.59E+12	3.98E+11	7.02E+11	7.69E+12
1.025	1.48E+12	3.62E+11	6.57E+11	7.22E+12
1.035	1.36E+12	3.41E+11	6.23E+11	7.05E+12
1.045	1.24E+12	3.14E+11	5.65E+11	6.61E+12
1.055	1.15E+12	2.80E+11	5.04E+11	6.30E+12
1.065	1.05E+12	2.50E+11	4.73E+11	6.07E+12
1.075	9.25E+11	2.31E+11	4.45E+11	5.77E+12
1.085	8.50E+11	2.23E+11	3.95E+11	5.46E+12
1.095	8.04E+11	1.93E+11	3.64E+11	5.21E+12
1.105	7.56E+11	1.75E+11	3.45E+11	4.86E+12
1.115	6.86E+11	1.63E+11	3.08E+11	4.72E+12
1.125	6.07E+11	1.45E+11	2.80E+11	4.40E+12
1.135	5.35E+11	1.35E+11	2.51E+11	4.22E+12
1.145	5.08E+11	1.22E+11	2.31E+11	4.04E+12
1.155	4.66E+11	1.11E+11	2.18E+11	3.86E+12
1.165	4.36E+11	1.04E+11	1.97E+11	3.62E+12
1.175	4.05E+11	9.64E+10	1.71E+11	3.42E+12
1.185	3.81E+11	8.98E+10	1.71E+11	3.24E+12
1.195	3.63E+11	8.44E+10	1.58E+11	3.04E+12
1.205	3.24E+11	7.42E+10	1.45E+11	2.90E+12

1.215	2.98E+11	7.33E+10	1.31E+11	2.77E+12
1.225	2.81E+11	6.80E+10	1.32E+11	2.71E+12
1.235	2.54E+11	5.62E+10	1.15E+11	2.54E+12
1.245	2.25E+11	5.51E+10	1.04E+11	2.44E+12
1.255	2.16E+11	5.10E+10	1.03E+11	2.31E+12
1.265	2.03E+11	4.74E+10	9.23E+10	2.21E+12
1.275	1.84E+11	4.47E+10	9.07E+10	2.07E+12
1.285	1.68E+11	3.74E+10	7.88E+10	1.99E+12
1.295	1.50E+11	3.47E+10	7.00E+10	1.94E+12
1.305	1.41E+11	3.10E+10	5.65E+10	1.78E+12
1.315	1.26E+11	3.11E+10	5.65E+10	1.68E+12
1.325	1.27E+11	2.76E+10	5.64E+10	1.61E+12
1.335	1.20E+11	2.40E+10	5.37E+10	1.51E+12
1.345	1.07E+11	2.75E+10	4.62E+10	1.40E+12
1.355	9.42E+10	2.41E+10	4.36E+10	1.35E+12
1.365	8.90E+10	2.54E+10	4.01E+10	1.27E+12
1.375	8.77E+10	2.56E+10	3.93E+10	1.25E+12
1.385	8.55E+10	1.95E+10	3.61E+10	1.17E+12
1.395	7.35E+10	1.65E+10	2.80E+10	1.12E+12
1.405	6.42E+10	2.05E+10	2.49E+10	1.08E+12
1.415	6.27E+10	1.45E+10	2.73E+10	1.03E+12
1.425	6.13E+10	1.19E+10	2.55E+10	9.89E+11
1.435	5.21E+10	1.25E+10	2.43E+10	9.32E+11
1.445	4.96E+10	9.19E+09	1.99E+10	8.66E+11
1.455	4.52E+10	9.45E+09	2.20E+10	8.55E+11
1.465	4.21E+10	7.70E+09	1.82E+10	8.06E+11
1.475	3.59E+10	6.04E+09	1.93E+10	7.64E+11
1.485	3.76E+10	6.20E+09	1.64E+10	7.28E+11
1.495	3.18E+10	4.92E+09	1.26E+10	6.83E+11
1.505	2.92E+10	6.43E+09	1.12E+10	6.66E+11
1.515	2.61E+10	4.69E+09	1.07E+10	6.01E+11
1.525	2.23E+10	6.21E+09	9.70E+09	5.75E+11
1.535	1.92E+10	4.99E+09	7.11E+09	5.46E+11
1.545	1.63E+10	3.94E+09	7.81E+09	5.12E+11
1.555	1.43E+10	3.39E+09	6.32E+09	4.81E+11
1.565	1.11E+10	3.26E+09	5.91E+09	4.40E+11
1.575	1.24E+10	2.71E+09	4.30E+09	4.31E+11
1.585	9.10E+09	1.18E+09	4.77E+09	4.05E+11
1.595	6.49E+09	2.11E+09	3.83E+09	3.45E+11

Table B.1: Average neutron and gamma flux values inside domain 1

C

MATLab code

C.1. Density calculations

```
clc;
clear all;

ConU=310;
mp235=20;
mp234=8.44e-3*mp235-7.0084e-4;
mp238=100-mp235-mp234;
w234=mp234/100;
w235=mp235/100;
w238=mp238/100;
Na=6.0221e23;
A234=234.0409522088;
A235=235.0439299;
A238=238.05078825;
rhoFuel=2.807;
B234=234+8*15.994+2*14.0067;
B235=235+8*15.994+2*14.0067;
B238=238+8*15.994+2*14.0067;
N234=(Na*(w234*ConU)/A234)/1000;
N235=(Na*(w235*ConU)/A235)/1000;
N238=(Na*(w238*ConU)/A238)/1000;
mFuel=(((N234*B234)/Na)+((N235*B235)/Na)+((N238*B238)/Na))*1000;
vFuel=mFuel/rhoFuel;
vWater=1000-vFuel;
rhoavg=(rhoFuel*vFuel+vWater)/(vFuel+vWater);
```

C.2. Heat capacity calculations

```
clear all;
close all;
clc;


y=[0.894 .759 .757 .646 .573 .574 .583 .530 .542 .493 .521 .513]*4.184;
x=[11.8 25.9 26.2 39.3 46.75 47.2 47.4 52.4 52.7 55.5 55.6 56.0];
ConU=25;
m=ConU/(238/(238+8*15.994+2*14.0067));
mp=(m/(m+1000))*100;
P=polyfit(x,y,1);
Heatcapacity=(P(1)*mp+P(2))
x2=[0:0.1:60];
y2=(P(1)*x2+P(2));
hFig = figure(1);
set(hFig, 'Position', [300 200 800 550])
plot(x,y,'+',x2,y2,'r')
a(1)=xlabel('Mass percentage uranium');
a(2)=ylabel('C_p [\frac{J}{gK}]');
a(3)=title('Heat capacity C_p v. UO_3(NO_3)_2 salt concentration');
a(4)=legend('Data from Literature','Linear Fit');
set(a,'Interpreter','latex','fontsize',12);
set(a(3),'Fontsize',12)
```